Don’t Breathe on Me

Modeling the Spread of Infectious Particles in an Elevator

Rae Brigham, Meghana Machireddy, Yohan Sequeira

Keywords: Computational fluid dynamics, COMSOL, Particle tracking, Airborne Disease Transmission, SARS

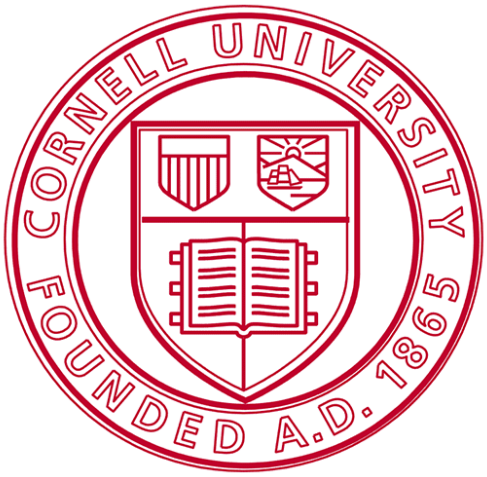

BEE 4530: Computer-Aided Engineering | Applications to Biological Processes
Cornell University

Table of Contents

1. Executive Summary

The contamination of surfaces in public spaces is of great importance to minimizing disease spread. When a large number of people share public spaces in close proximity, aerial disease transmission becomes common, especially in enclosed spaces such as small rooms and elevators. An understanding of disease-carrying particle deposition from breathing and airflow is a vital step in determining how to prevent the spread of disease in confined public spaces.

Previously, studies have modelled the airflow in larger structures such as airplanes and rooms where the airflow is predetermined due to the presence of central ventilation. These models combine the airflow from vents and human sources to study the deposition of particles on surfaces (Tang et al., 2013; Yan, Li, Shang, & Tu, 2017; Zhao, Zhang, & Li, 2005). Similarly, this model incorporates ventilation and human breathing inside of an elevator to determine final particle spread and deposition. This model will determine what factors determine the spread and deposition of particles in an elevator. For example, this model will test whether the flow of air caused by the vents in the elevator is the dominant factor determining the dispersion of particles, or whether breathing air velocity is more important to particle spread.

To test these parameters, a 3D model was developed of a standard elevator with a vent input two feet to the left of the center of the elevator and a vent exhaust two feet to the right of the center which follows the model found in most elevators. Using the ASME standard for elevator ventilation it was determined that the flow of air into and out of the elevator occurs at an equal rate of 5 $L/(s*m^2)$ (2105 code). Finally, a sine function was created with an amplitude of 1.3 m/s that modeled the breathing velocity of a human subject inside the elevator based on average breathing velocities found in literature (Tang et al., 2013; Yan et al., 2017).

After running the model to solve for the laminar flow fluid dynamics, Lagrangian particle tracking (using Stokes drag law) was simulated for a maximum time period of 500 seconds. Using this initial model, a sensitivity analysis was done by varying the breathing function to simulate shallow and deep breaths as well as varying the location of the person around the elevator. The solution was validated by comparing with data from a study done by Tang. et. al in 2013, as well as with experimental data derived from thermal images of breath propagation.

The results indicate that the patterns of propagation throughout time were turbulent in the normal solution, and involved the particles moving toward the vent and then being caught in an eddy-like backflow. The particle trajectories varied significantly from this trajectory as parameters such as the breathing velocity, source position and inlet velocity were changed. This indicates that the location of body within the elevator as well as the velocity of breath have significant impacts on the fluid dynamics within the elevator, as well as the amount of time that the disease particles circulate before coming to rest or flowing out through the vents. When the body

position is close to the vent, or the vent velocities are higher, the particles are sucked into the outlet vent faster compared to the control. These results indicate that minimizing particle spread and disease transmission in elevators can be accomplished by designing elevators with higher numbers of vents and higher inlet vent velocities.

Keywords: Computational fluid dynamics, COMSOL, Particle tracking, Airborne Disease Transmission, SARS

2. Introduction

Reduction of viral particles in public areas has been attempted by design standards and public safety mandates over the last century, with most of this effort focusing on surface contamination. Through research and the development of antibacterial surfaces and sanitary practices, the spread of disease through surface contact has decreased (Nazaroff & Cass, 1989). Despite this, there has been a growing concern about the spread of contagious disease through the air; specifically the highly contagious and fatal diseases for which the population has no immunity. In these cases, the best way to reduce the impact of such a disease is by limiting the spread of disease by reducing contamination (Jones & Brosseau, 2015). One example of such a disease is Severe Acute Respiratory Syndrome (SARS). SARS has been a factor of great concern to governments and the healthcare industry due to its resistance to treatment and high rates of contamination from a single point source (Christian et al., 2004). During a SARS outbreak in 2003, it was found that the main factor leading to disease transmission was the contamination of a Boeing-737 carrying an infected passenger (Yan et al., 2017). In a 2017 study led by researchers at RMIT University, the aerosol particle spread in a Boeing-737 was modeled through particle tracking and fluid flow(Yan et al., 2017). They found a large contamination risk to passengers sitting within one to two rows of the infected individual. This was exacerbated by the enclosed nature of the airplane's ventilation system, as well as the long period of time that passengers are near each other. The danger of an infectious event of this scale was also increased by the large number of people that passed through the airline cabin in a short amount of time, and the fact that the flight in question connected large densely populated cities (Yan et al., 2017). To minimize the risks of similar events, further study of disease transmission in enclosed and highly trafficked spaces is needed.

To this end, the system of research being analyzed in this study is an elevator car. This is an enclosed and public space that has not been greatly studied with regards to aerial disease transmission. A 2015 study estimated there to be 7 billion elevator trips daily around the globe (Al-Kodmany, 2015). Furthermore, elevators, like airplanes, are confined spaces with predetermined ventilation where particles can accumulate if the fluid exchange rate is insufficient. In fact, a 2014 study by Kandel et. al found that elevator control panels had higher

incidences of bacterial contamination than public toilet seats (Kandel, Simor, & Redelmeier, 2014). Throughout these studies, it has been established that elevator cars can be hotbeds for disease due to their public nature, intense use and traffic, and confined airflow (Al-Kodmany, 2015; Kandel et al., 2014). Despite this, there is little research that addresses aerosol contamination and deposition of particles in elevators.

This study primarily aims to model the dispersion of viral vectors like SARS from a single point source within a standard elevator car. It aims to identify the factors that most influence the spread of disease vectors within a confined space, including as inlet vent velocity, source position and particle size. While most current research focuses on contaminant deposition on surfaces, this paper wishes to further research into aerial contamination through disease carrying particles, and the specific configuration of variables that affect these particles trajectory and final deposition pattern.

The dispersion of SARS-like particles will be modeled by assuming a primary particle diameter of 1.8 μm and applying the Navier-Stokes equations in 3 dimensions and Lagrangian Particle Tracking. The Navier-Stokes equations will first be used to simulate the air flow in the elevator caused by the ventilation as well as breathing. This velocity field solution will then be used as an input to the Lagrangian particle tracking, which will be used to calculate the particle positions and velocities by coupling the fluid velocity with Stoke's drag law. The source of contamination will be modeled as a time-dependent exhale, with a max velocity of 1.3 $\frac{m}{s}$ and a sinusoidal pattern. Particles will be released at multiple points along this sinusoid in order to create a life-like breathing pattern.

The model of elevator cab chosen is a 2 m by 2 m square cab that stands 2.5 m tall. The effects of door opening/closing, and motion of the box itself are neglected to simplify the problem. For ventilation, one vent and one outlet are modeled on the ceiling of the elevator. According to ASME design standards, elevator ventilation usually occurs at a rate of 5 $\frac{L}{m^2 * s}$ Therefore, the vent in the model will have an initial forced velocity of 0.7 $\frac{m}{s}$ (International Mechanical Code, 2015).

By analyzing the typical patterns of dispersion of disease carrying vectors within a confined space, a better understanding the spatial variables that impact disease spread in confined public spaces can be gained, and eventually this information could be used to reduce contamination. This could have growing importance in the future as viral agents continue to evolve and airborne illnesses become a global health issue of increasing concern.

Design Objectives:

Disease carrying particles are deposited in elevators through airflow from human breathing. The objective of this model is to study the effect of certain parameters in this phenomena including; source location, particle size, inlet velocity and breathing velocity on the final dispersion of particles in the elevator. Through the course of this research the goals include:

1. Develop a model that can describe the airflow in a way that is consistent with other models of airflow in enclosed spaces.
2. Design the model such that parameters such as size of the particle, the position of particle source, and airflow velocities can be varied.
3. Determine a combination of model parameters that result in a reduction of particle circulation.
4. Analyze the parameters of the model to determine which will have the greatest effect on the final spread of particles.
5. Recommend design considerations for elevators to minimize particle spread and reduce contamination.

3. Methods

Schematics:

The schematic describes what can be interpreted as a 'typical' elevator. The basic geometry for the elevator was created using the ASME guidelines for compliance standards in the United States (International Building Code, 2012). The schematic includes an inlet vent in the upper right corner of the ceiling, an outlet vent in the lower left corner of the ceiling. The simulated person (who is emitting the particles) is centered around the point $(X,Y) = (1, 0.5)$ m, and is facing towards the wall closest to the outlet vent. The dimensions and the boundary conditions of our model are illustrated below:

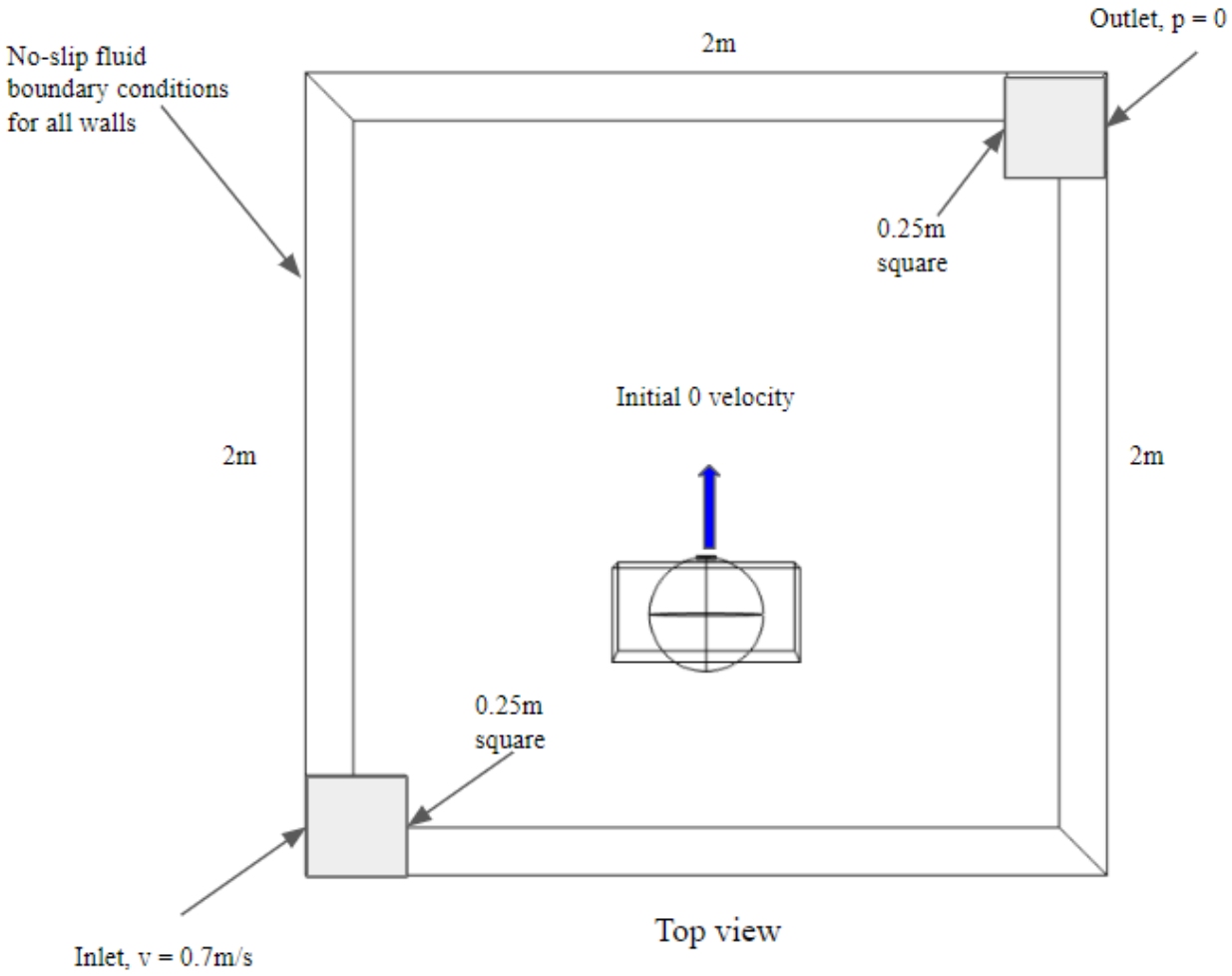

Figure 1: Top view of the elevator geometry. This geometry was created to be the most simple (and smallest by absolute volume), but realistic elevator geometry possible. This was done to reduce computation time while still preserving the physical accuracy of our model.

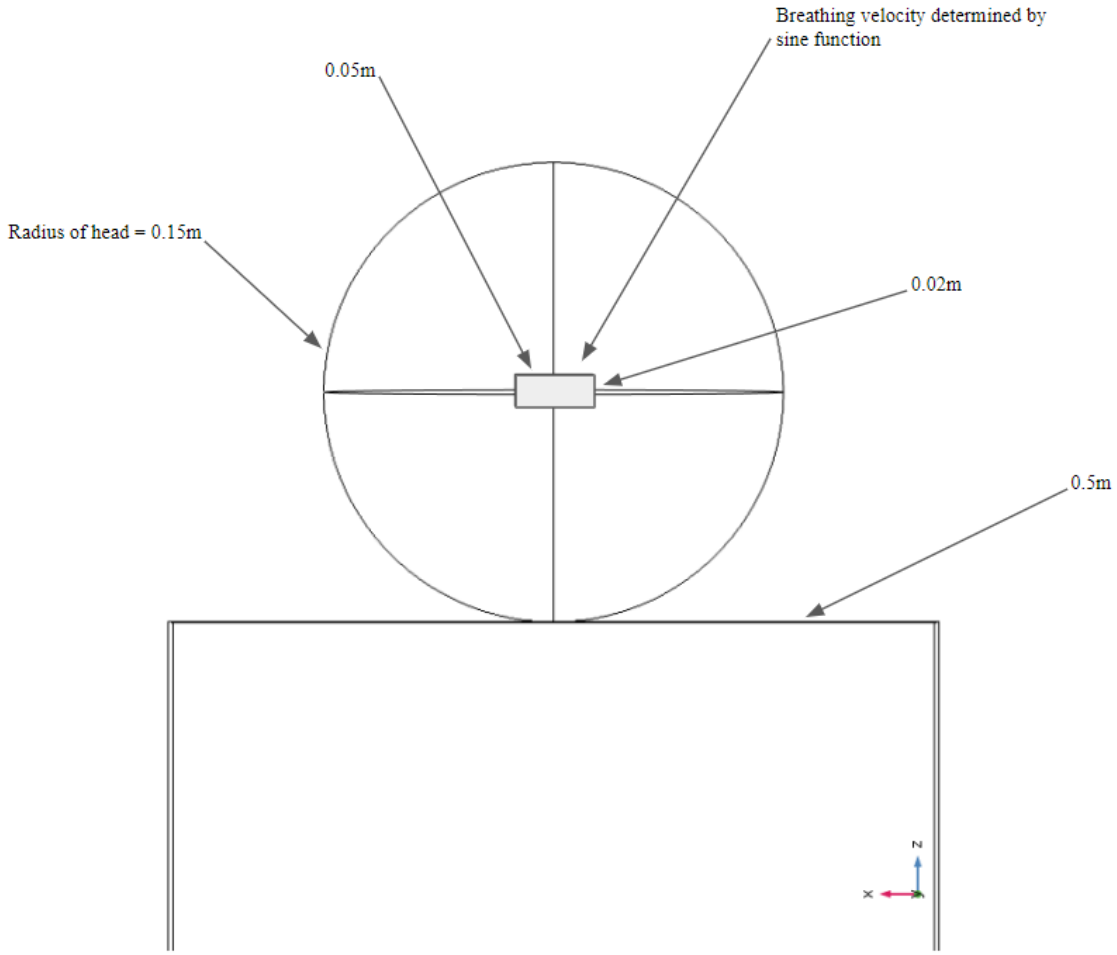

Figure 2: Front View of simplified person. The geometry for the person was vastly simplified to the bare minimum geometry that would affect fluid flow. This simplification allowed the mesh to be less skewed, and maintained a more reasonable ratio between the sizes of the mesh elements.

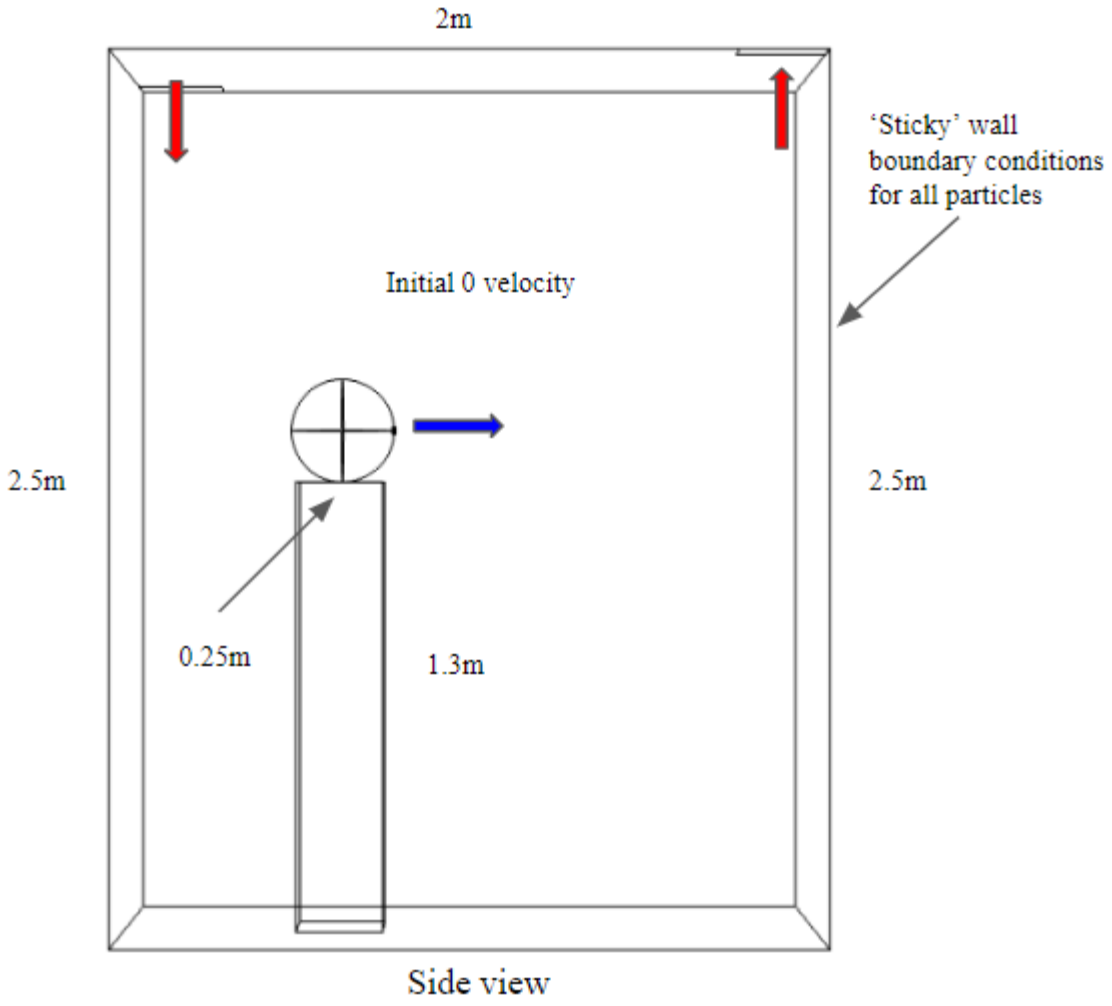

Figure 3: Side view of person. The position of the person in the elevator in this diagram was taken as the 'normal' or default position, however our analysis takes into account several source positions. The height and dimensions of the person in the elevator were taken from average values for US male height (Fryar, Kruszon-Moran, Gu, & Ogden, 2018).

Note that the inlet vent velocity is set at $0.7\ \frac{m}{s}$ (directly downwards) for the control case and the walls have no slip boundary conditions for fluid flow and are sticky for particle tracking. The outlet boundary condition is set as a zero pressure boundary condition, but it is in essence undefined as it is part of the solution calculated by COMSOL according to the continuity equation.

This model also simulates breathing at the mouth. To represent a periodic inhale and exhale, the inlet velocity was simulated by using a sine function with a maximum velocity of 1.3 $\frac{m}{s}$ and a period of 4 seconds. The function is plotted below:

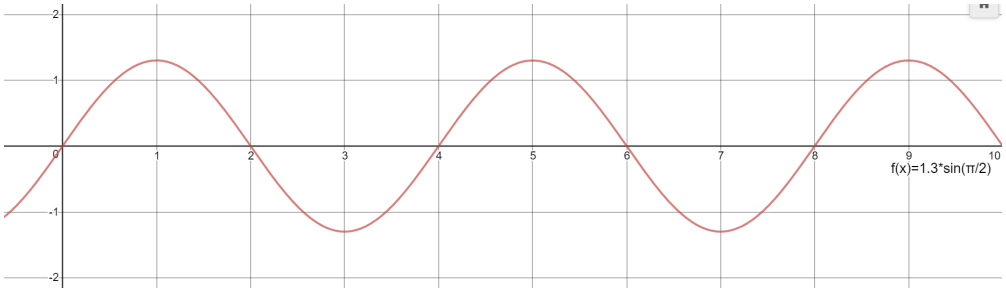

Figure 4: Breathing function ($\frac{m}{s}$). The sinusoidal breathing function was created based on the breathing function used by Zhao et al. in their 2003 study that modeled human breathing in an enclosed space (Zhao et al., 2005). Note that the negative portion of the sine curve represents breathing in, and is reflected in the inlet velocities by a negative velocity (fluid flow towards the mouth instead of away). The maximum velocity of 1.3 $\frac{m}{s}$ was taken from a study by Tang et. al. in 2013 which studied particle propagation through breathing (Tang et al., 2013).

Mesh Convergence:

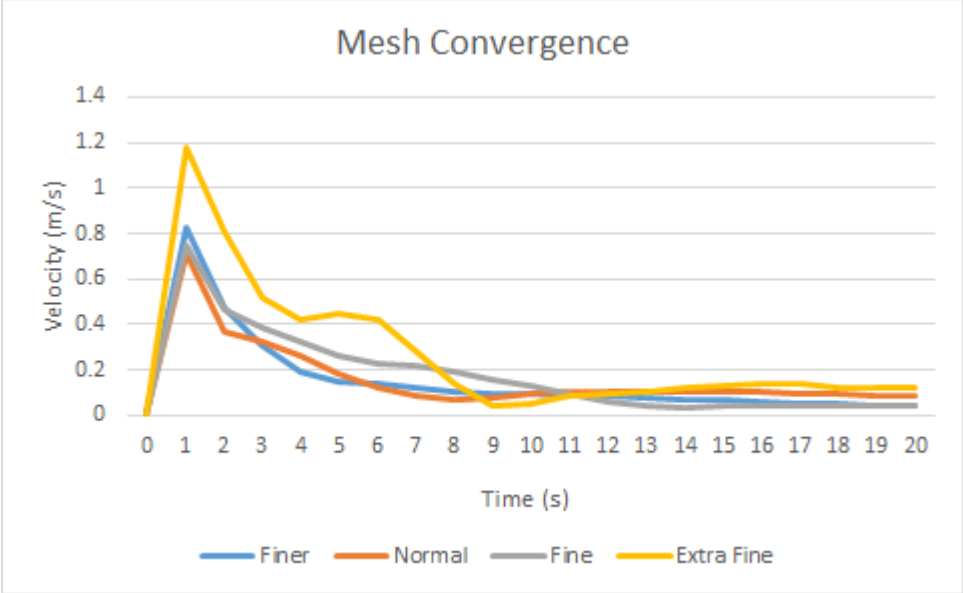

Figure 5: Velocity vs. Time for different mesh sizes at the point (1, 1, 1). This point was chosen as a point in the center of the computational space, and as a point that would be affected by both the vent velocity and the breathing pattern.

As seen by the mesh convergence in Figure 5, after an initial period of high variation due to preliminary solver instability, the variation of element size causes a maximum of .2 $\frac{m}{s}$ change in velocity for normal-extra fine mesh values. Because of this, the initial computations were performed using an "Extra Fine" mesh (280707 elements) for maximum accuracy, but the sensitivity analysis was performed using a "Fine" mesh (28919 elements) to save computational time. Since the particles will be released starting at 40 seconds, the variability of velocity values of the solution before the solution stabilizes around 10-30 seconds do not affect our final results. This is confirmed with the below plot, showing the y velocity pattern in front of the mouth for times after 30 seconds.

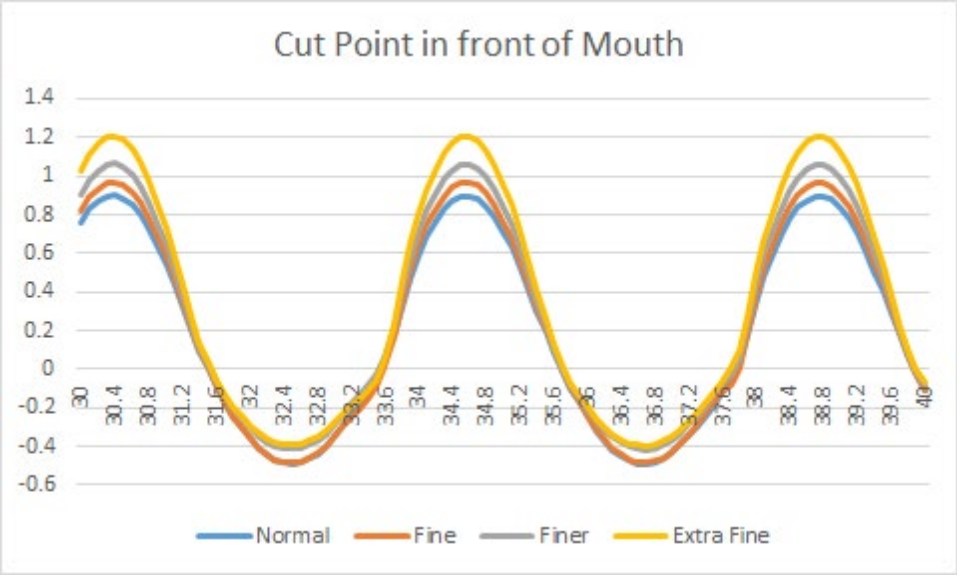

Figure 6: Y-velocity over time at cut point (Appendix Figure 2) for different mesh sizes. Even though the maximum value for velocity is slightly different at the peak velocities, the majority of the velocity solutions for different mesh sizes are the same values. Considering that the particles are also released at many times along the curve, it is reasonable to use a fine mesh for sensitivity analysis. This also drastically reduces computation time.

Figure 6 shows that though the maximum and minimum values of the breathing function vary with decreasing element size, the period and frequency remain constant. As the model endeavors to study the effects of various parameter variations on particle distribution over time, the value of the particle velocity at any single point is not as important to the study as the change in velocity due to parameter variation. Additionally, as the particles are released at nine different points on the sine curve, the maximum and minimum velocity values would likely only affect a small subset of the particles released: those near 90 degrees. The maximum difference in velocity values between the two element sizes was also .2 $\frac{m}{s}$, or 17% of the average maximum value at the cut point, indicating that the difference is small enough to be ignored for sensitivity analysis.

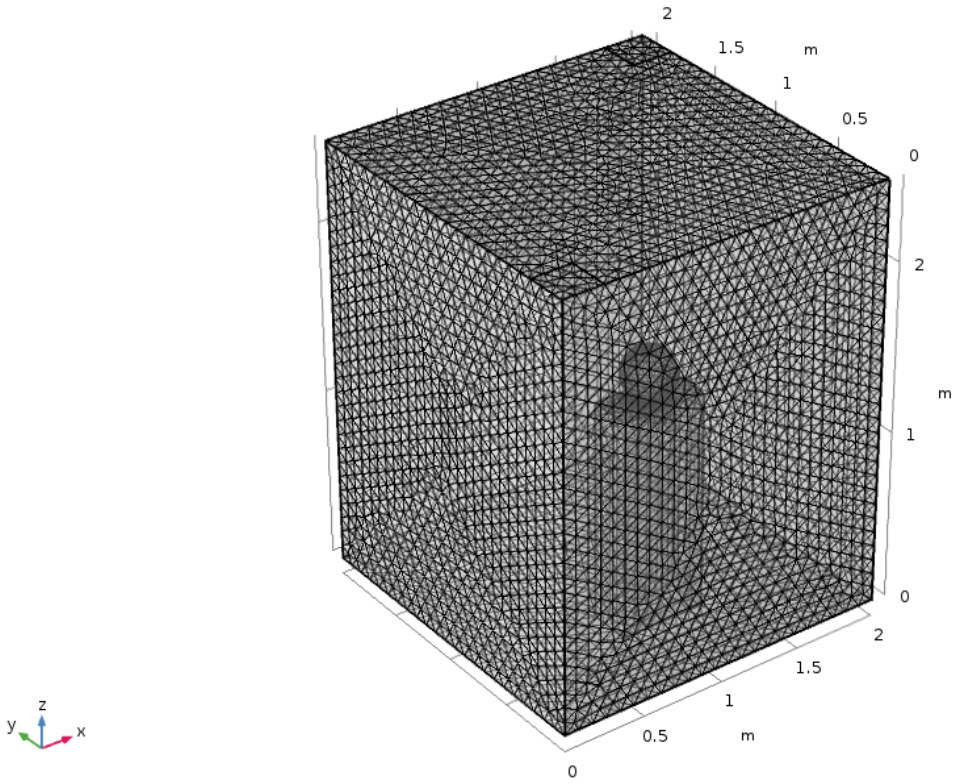

Figure 7: The final fully meshed model of the system (Extra Fine element size). The mesh consisted of 280707 tetrahedral elements.

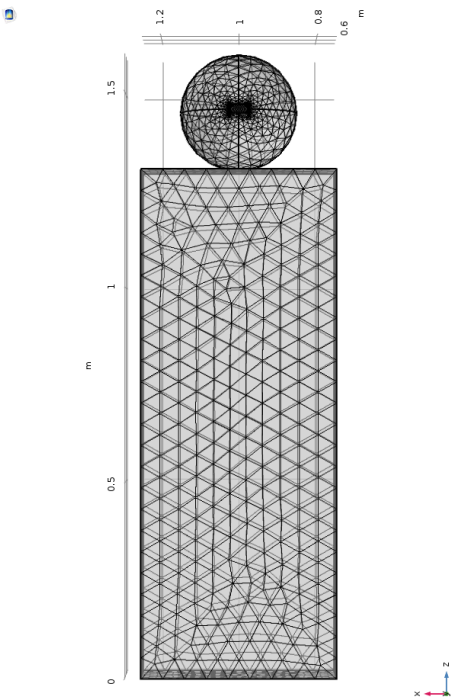

Figure 8: The final mesh of the simplified person geometry (normal element size). Note the small mesh elements near the mouth.

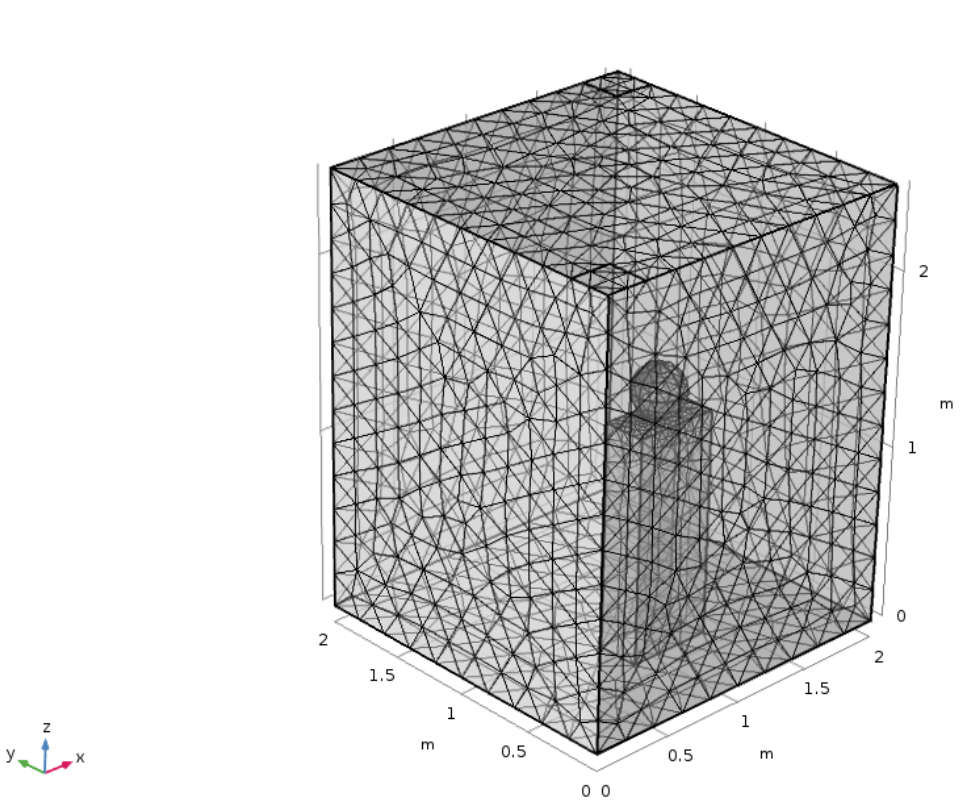

Figure 9: The final mesh for sensitivity analysis (fine element size). The mesh contained 28919 elements.

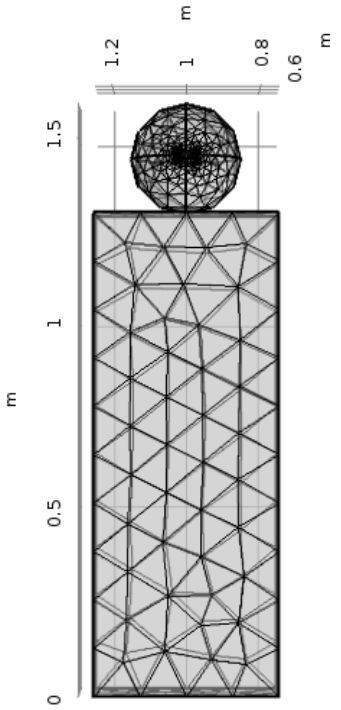

Figure 10: The final mesh body for sensitivity analysis (fine element size). While the rectangular body of the person was meshed fairly accurately, the head specifically suffers from some small discretization error as the tetrahedral shapes approximate the spherical head geometry.

Governing equations:

To reduce computation time and simplify the solution, this model ignores thermal effects (assuming their contribution to the flow to be minimal) as well turbulent flow and other physical effects. This simplified model includes physics for laminar isothermal fluid flow and Lagrangian particle tracking. The model ignores the effects of particle evaporation and other physical effects to simplify computation. The model uses the Navier-Stokes equations (in three dimensions), and the Lagrangian equations for particle tracking shown below.

$$\rho \nabla V = 0 \qquad (1)$$

Equation 1: The continuity equation. This equation is solved with Navier-Stokes, and describes the conservation of mass in the system (the elevator). V is the velocity and ρ is the fluid density.

$$p\left[\frac{\partial V}{\partial t} + (V \cdot \nabla)V\right] = -\nabla P + \rho g + \mu \nabla^2 V \quad (2)$$

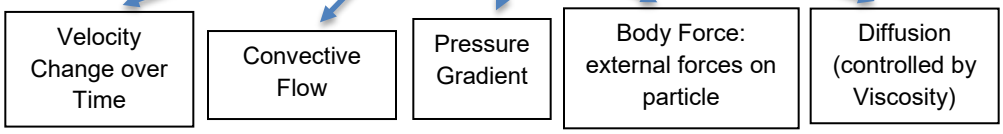

Equation 2: Navier-Stokes equations for three-dimensional flow. This system used Navier-Stokes for three dimensional flow, thus keeping all the terms in the equation (equation shown in vector form). P is the fluid pressure, ρ is the fluid density, μ is the fluid viscosity, v is the velocity, and g is the gravitational constant.

$$F_\tau = \frac{d(m_\rho v)}{dt} \quad (3)$$

Equation 3: Lagrangian particle tracking. This equation relates the change in velocity of the particle, to the forces experienced by the particle (essentially Newton's second law). V is the particle velocity, m_p is the mass of the particle and F_t is the sum of forces on the particle

$$F_g = m_\rho g \frac{(\rho_p - \rho)}{\rho_p} \quad (4)$$

Equation 4: The gravity force experienced by the particle. F_g is the gravitational force, m_p is the mass of the particle, ρ_p is the density of the particle, ρ is the density of the fluid and g is the gravitational constant.

$$F_D = \frac{1}{\tau_p} m_p (u - v) \quad (5)$$

$$\tau_p = \frac{\rho_p d_p^2}{18\mu} \quad (6)$$

Equations 5-6: The drag force experienced by the particle (incorporating Stokes drag law). This drag force equation incorporates $\tau\rho$ which is a value calculated from the particle diameter (d_p) as well as other fluid constants. The u and v terms in the equation refer to the fluid and particle velocities respectively.

All additional standard properties used in the equations initially such as particle properties, air properties and physical constants are defined in Table 1 in the Appendix.

4. Results

Initially, the model was run for 500 seconds with 5 particles released at 9 separate times. The particle releases were timed so that they coincided with the positive half of a single breathing cycle beginning at 40 seconds, and plotted below for clarity.

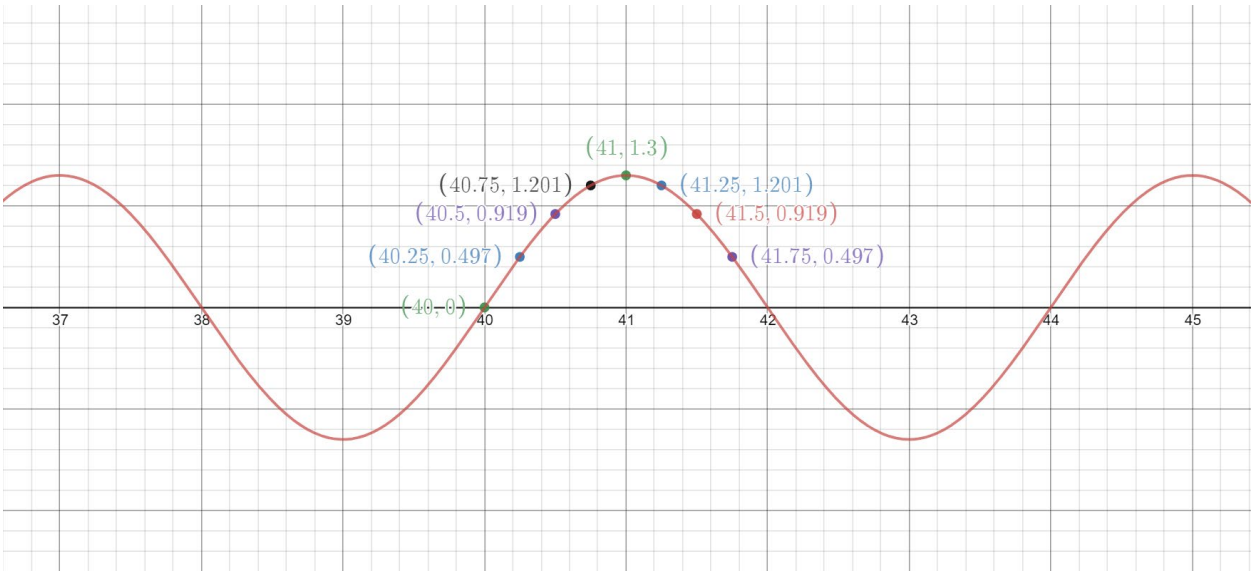

Figure 12: Particle release times for the initial model. The particles were released along the positive phase of the sine curve to simulate a full breath. Note that the release time is around 40 seconds, postponed to allow time for the solution to stabilize.

To verify that the breathing at the mouth was occurring with the correct frequency and amplitude, a cut point 3D plot was taken with the point defined just in front of the center of the mouth. The velocity of the fluid (y-component) was recorded at this point, to verify if the breathing pattern was accurate to what was set as the mouth input velocity (Fig. 12).

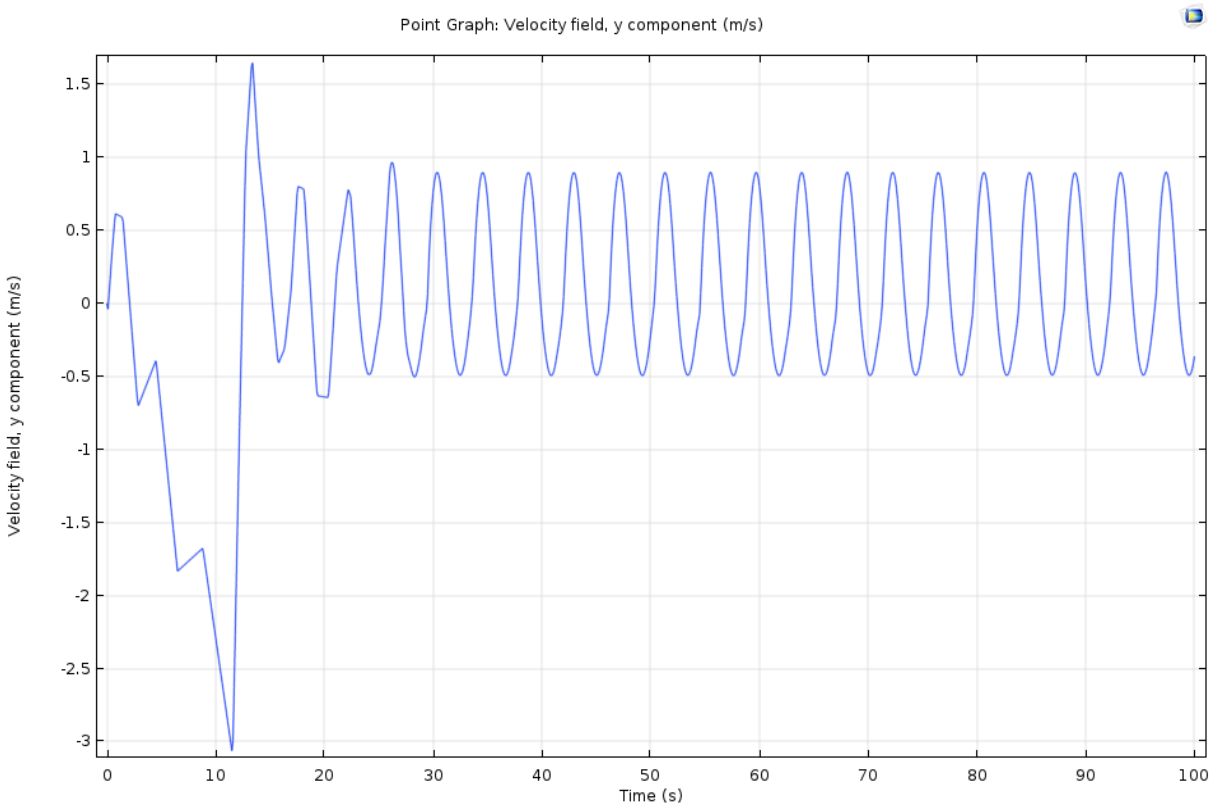

Figure 13: Fluid velocity just in front of the center of the mouth, y-component. The breathing function stabilized after approximately 30 seconds.

The function in Fig. 13 after it stabilizes around 30 seconds corroborates the validity of the solution as it shows a similar period and amplitude to the original breathing function (Fig. 12).

The fluid flow computation was run for a period of 100 seconds with particle release at 40 seconds. For particle tracking, the velocity at times past 100 seconds was interpolated from the stabilized solution, and the particles circulated for 500 seconds. This was done for two reasons. Firstly, the effect of breathing on the particle trajectories (and overall fluid flow) is only significant when the particles are very close to the mouth (when the particles are released). Because the particle release occurs at 40 seconds, and the particles are close to the mouth for only another 20-30 seconds, after about 70 seconds the particle trajectories are only determined by the 'steady-state' fluid flow. This is why it is valid to interpolate the 'steady-state' solution for 100 seconds over the next 400 seconds. The second reason that this interpolation was done was to reduce computational time, as running laminar flow for 100 seconds already required significant computation time.

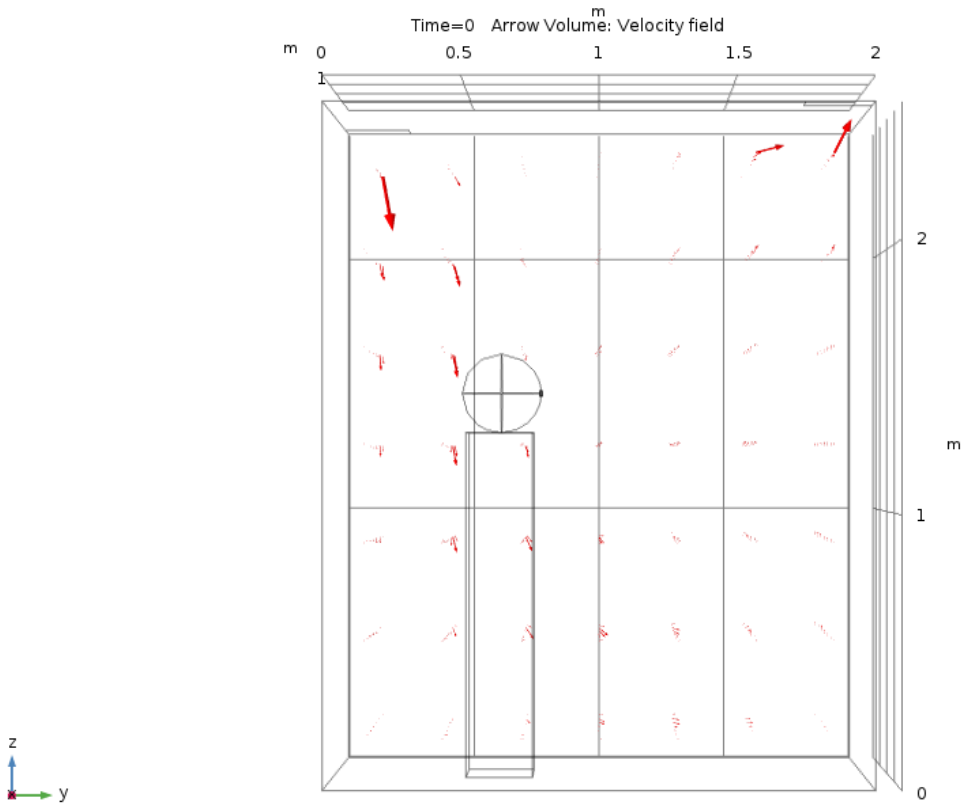

Figure 14: ‘Steady-state’ fluid flow solution, side view. The plot above shows the fluid flow solution, where the red arrows represent the direction and magnitude of fluid flow. Because the contribution to the overall flow by the mouth is so small, and the inlet has a constant velocity boundary condition, the flow essentially stabilizes to this solution. (note that while the time says 0 seconds, this is an interpolated value of the steady state flow, and not a snapshot of fluid flow taken from a time before the solution stabilizes)

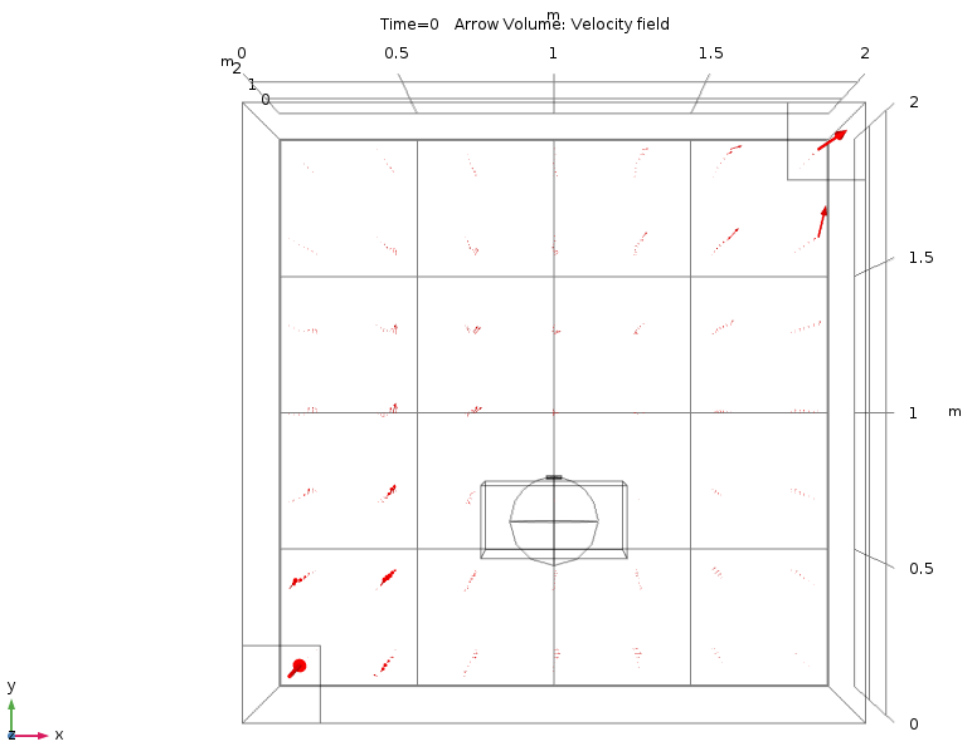

Figure 15: ‘Steady-state’ fluid flow solution, top view. Note the overall diagonal direction of the flow from inlet to outlet. (note that while the time says 0 seconds, this is an interpolated value of the steady state flow, and not a snapshot of fluid flow taken from a time before the solution stabilizes)

The second step in running the model was to run particle tracking. The particles were simulated for 500 seconds (after a release at 40 seconds). This was done to simulate the maximum possible length of elevator ride, but for the majority of short elevator trips, the useful data was collected from earlier times in the trajectory data. The particle distribution plots after 500 seconds with standard parameter values are shown below:

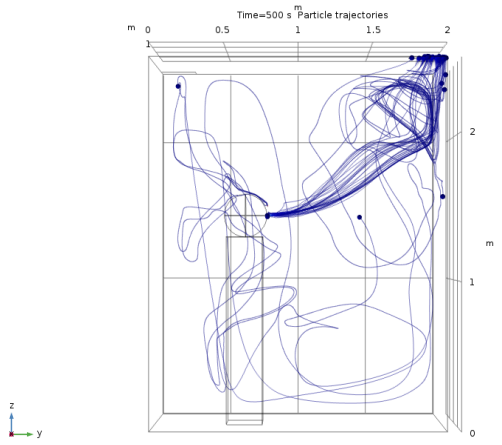

Figure 16a: Side view of particle trajectories

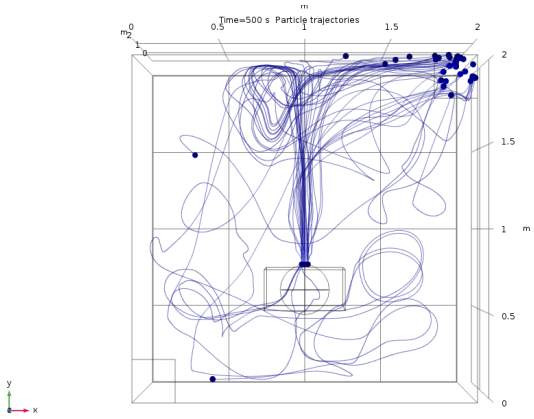

Figure 16b: Top view of particle trajectories

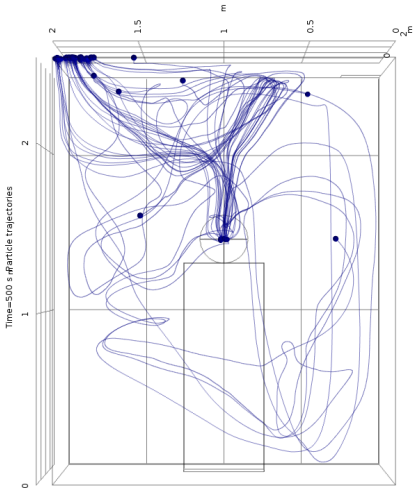

Figure 16c: Frontal view of particle trajectories

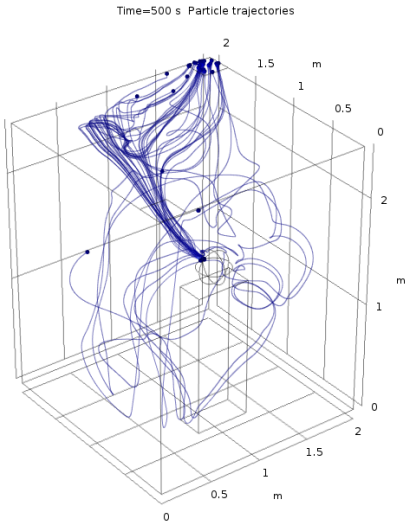

Figure 16d: Orthogonal view of particle trajectories

As seen in the plots above, the particles experienced significant turbulence after release. The particles propagate upwards and towards the wall in front of the mouth for the first 85 seconds, but as they near the wall they disperse and the flow pattern changes significantly. Some of the particles flow straight towards the outlet vent from the wall, though many are caught up in fluid

eddies and complexities that carry them away. After 500 seconds, many of the particles end up close to or on the outlet vent but some are still circulating the cabin. This result indicates that there is a significant turbulence pattern in the elevator causing initial updraft and backflow. A possible explanation for the variation in flow pattern could be the positioning of the person in the elevator. Because the person is a solid block, its presence disrupts the smoothness of the airflow from one vent to another. This disruption combined with the velocity gradient created by the mouth breathing function could explain some of the eddy characteristics observed in the above plots.

This phenomena can be further studied by isolating the breathing inlet from the influence of the overhead vent.

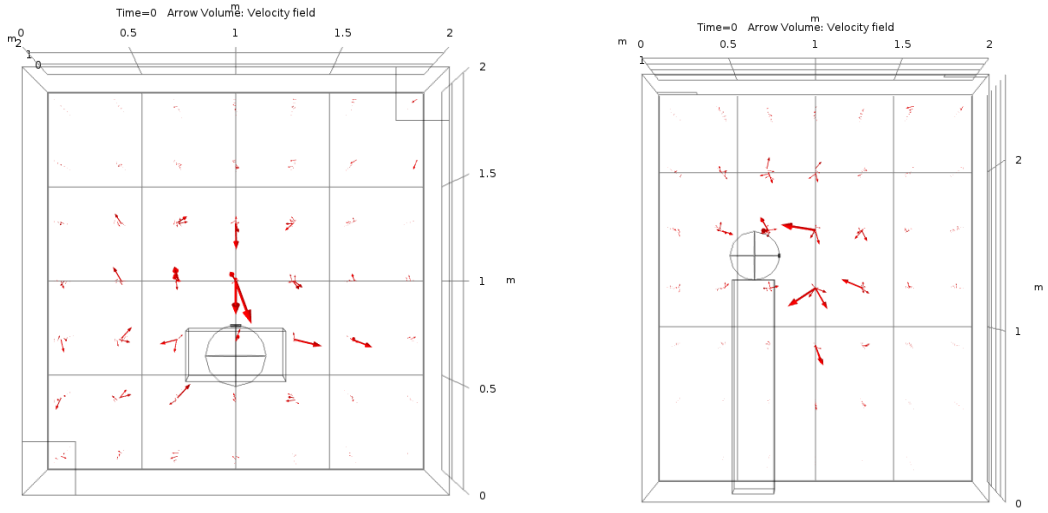

Figures 17a and 17b: Velocity arrow plots derived from just the breathing inlet velocity gradient. (note that while the time says 0 seconds, this is an interpolated value of the steady state flow, and not a snapshot of fluid flow taken from a time before the solution stabilizes)

As seen in Figures 17a and 17b, the breathing inlet itself causes strong circulatory currents that induce a backflow and eddy after an initial propagation distance. When the streamline plot for the combined effect of the inlet and breathing function is created, the disruptive impacts of the body and breathing function become clear.

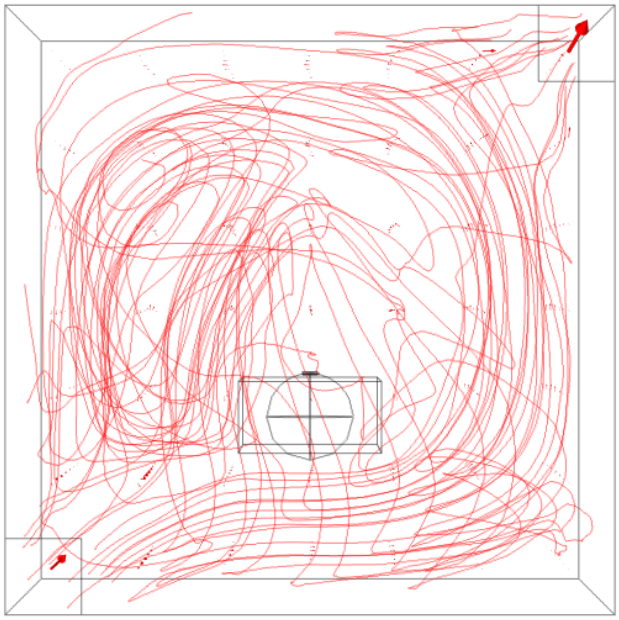

Figure 18: Velocity Streamline plot for particle tracking with vent and breathing inlets. While the plot is complex, the overall trend is still clear. The presence of a body disrupts the diagonal fluid flow and introduces fluid eddies and complicates the flow patterns.

The figure above shows the tendency of the particles to circulate close to the body and with increasing circulatory radius until they finally proceed towards the vent. Not only do the streamlines between the vents separate around the body, but the fluid behavior directly in front of the mouth exhibits circulatory behavior that introduces the particles released from the mouth into the flow of air between the vents. Together, these effects produce particle propagation patterns that begin straightforward, but over time begin to backflow over time and enlarge the volume of contaminated air in the room.

This phenomena has larger implications for disease spread--if the particles circulate for longer than the time they propagate straight ahead, the chance of infection in other passengers continues to increase with time rather than position being the determining variable. During long elevator rides the best way to minimize particle spread in this case would be to position the sick person closer to the vent, as opposed to maximizing distance between the sick individual and other passengers, as over time the particles will spread throughout the entire elevator regardless. The key factor seems to be the distance that the infected person is from the vent.

The distance and spread as a function of time of time is isolated to better understand the behavior of the particles over time of propagation by time after the release.

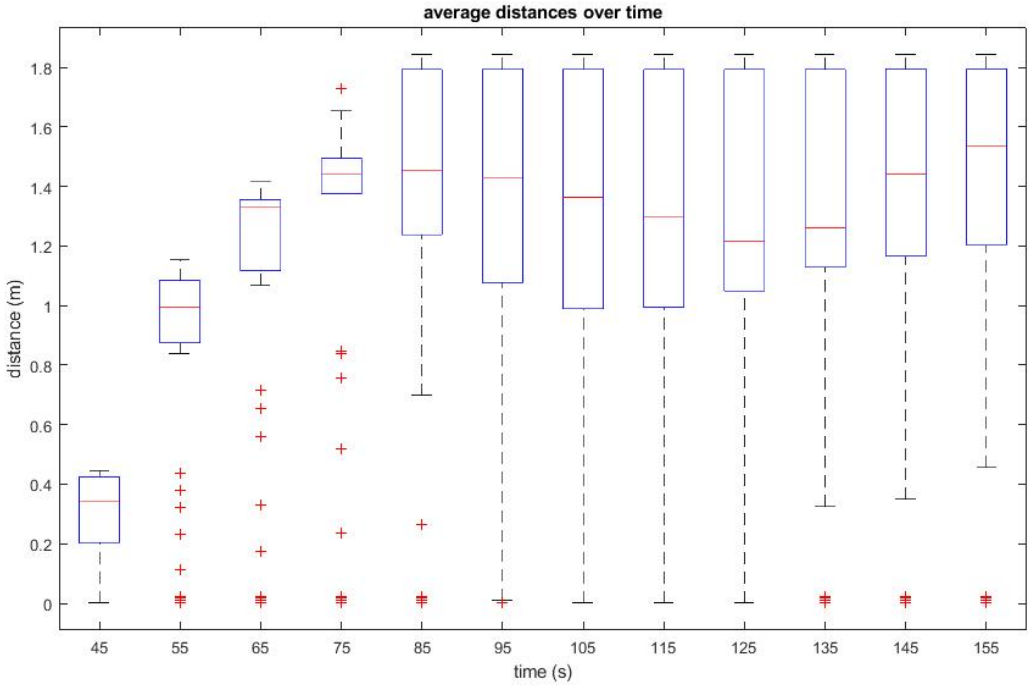

Figure 19: Average distance of propagation over time. The box plots show the maximum, minimum and average values for all particle distances over time. As shown above, the particles begin to spread after their release (around 85 seconds) and reach a maximum dispersion (or spread) around 110 seconds (with some small variation as the particles are drawn into eddies and more complex flow patterns)

As seen in Figure 19 and Figure 1 in the appendix, the propagation pattern of the particles over time is cyclical. The particles begin with a straightforward trajectory with little variation in distance among particles initially after release, but after about 80 seconds they begin to disperse and propagate in separate directions. This corresponds with the eddy and backflow pattern observed in Figures 16a-d. After 85 seconds, some of the particles begin to come to rest, with the distribution patterns widening but capping at a max distance of 1.8m from the mouth. The average distance of propagation is around 1, which indicates that the cloud of particles is still traveling primarily in a group. The max value of 1.8 meters corresponds to the distance between the mouth and the vent, indicating that the upper limit of the spread is reached when the particles stick at the outlet. After 110 seconds, the distribution of particles begins to narrow as the remaining circulating particles propagate towards the outlet vent as well.

Validation:

For validation, the computational data is compared to the work of Tang et al. who reported the maximum distance and area of the visible propagation of the particles from the individual's mouth. They found that, "For the breathing modalities, the maximum visible propagation distance and derived exhalation velocity for mouth breathing were 0.6 m and 1.4 m/s, respectively" (Tang et al., 2013). The associated plots are below:

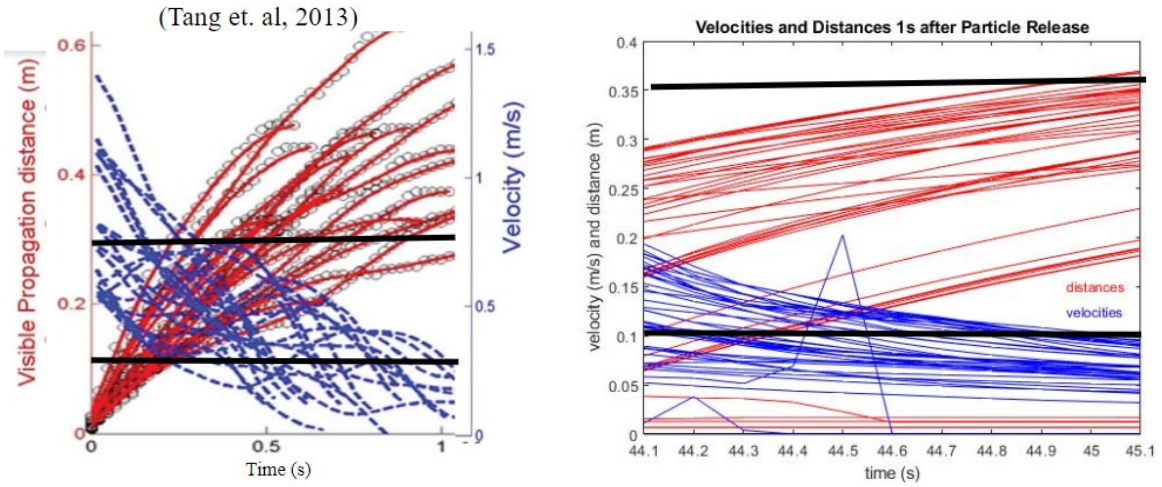

Figures 20a and 20b: Velocity and Distance of propagation immediately after release. Left to Right: (Tang et. al, 2013), COMSOL simulation. The black lines indicate equal values.

Figure 20a shows the distance and velocity curves of airborne particles immediately after release in a study by Tang et. al 2013. Values immediately after release were chosen for validation because this is when the particles would primarily experience the effects of the fluid flow created by breathing, and not experience additional fluid flow effects from the vents. It is at this time that the geometric complexity would be most like that modeled in Tang et. al. Figure 20b shows the distance and velocity curves of the particles in our model for 1 second after all of the particles are released. By comparing the two graphs, it is clear that the general trends in both graphs are similar. The particles in the model created by Tang et al. travel approximately 0.4 meters in the first 0.5 seconds whereas the particles in this model travelled approximately 0.2 m in the first 0.5 seconds. The velocities in the model created by Tang et al. begin at 0.2 $\frac{m}{s}$ and decelerate to 0.05 m/s whereas the particles in Figure 20b begin with an average velocity of approximately 0.15 m/s and decelerate to a velocity of 0.05 $\frac{m}{s}$. The differences in values between the Tang et. al study and this simulation can be attributed to changes in particle release, as well as the effect of multiple releases in the results simulation on propagation. Since the particles in this model are released at nine points along the breathing function, some of the particles would have slowed down before they appear on the graph, indicating that the actual starting velocity and distribution

of the particles would be higher and closer to the value reported by Tang et al. Furthermore, the particle release velocities in Tang et al. are slightly higher than in this model, which explains the higher velocity after 1 second as well as the higher dispersion. Due to the fairly small differences between the particle position and velocity data and the data from Tang et al. it is reasonable to say that this study provides a valid simulation of breathing and particle tracking.

To further validate the model images captured with a thermal imaging camera of a typical deep and shallow breathing pattern were used. The images were captured in a room with no significant ventilation to simplify the fluid flow as much as possible. To compare, the simulation was run using just the breathing source as an inlet (no vent) and the shallow and deep breathing functions as defined in Figure 21.

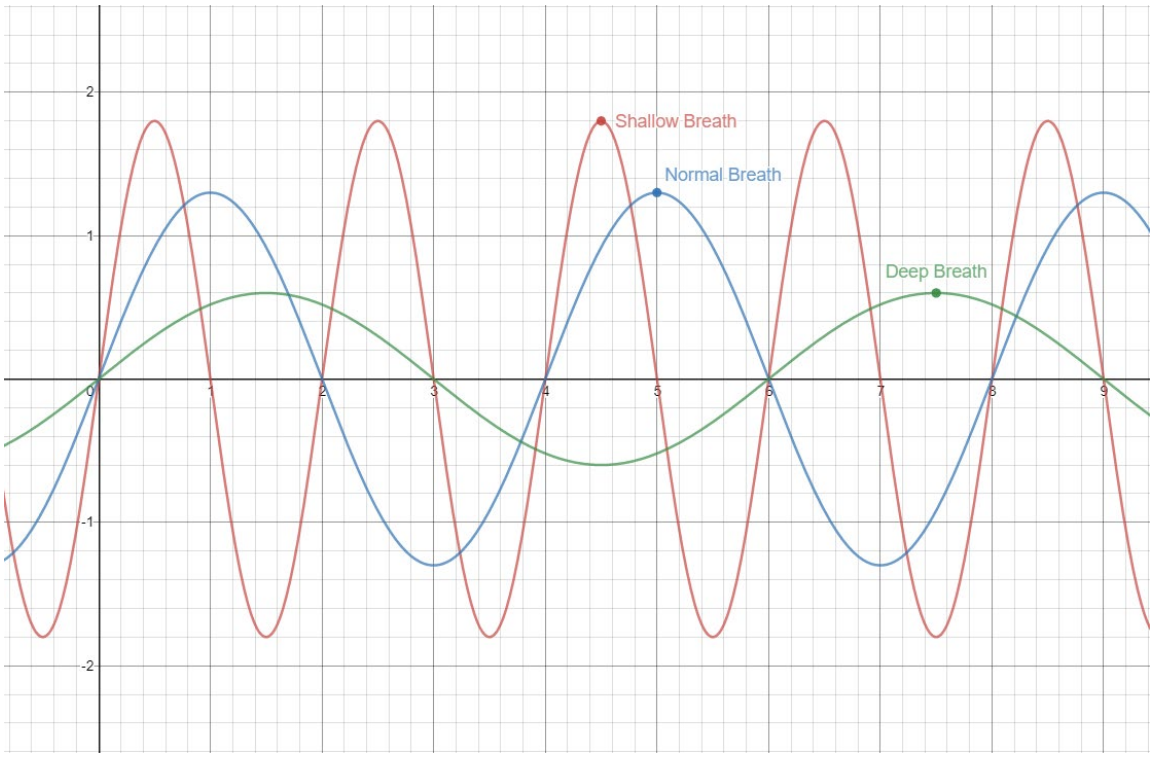

Figure 21: Shallow, Normal and Deep Breathing functions.

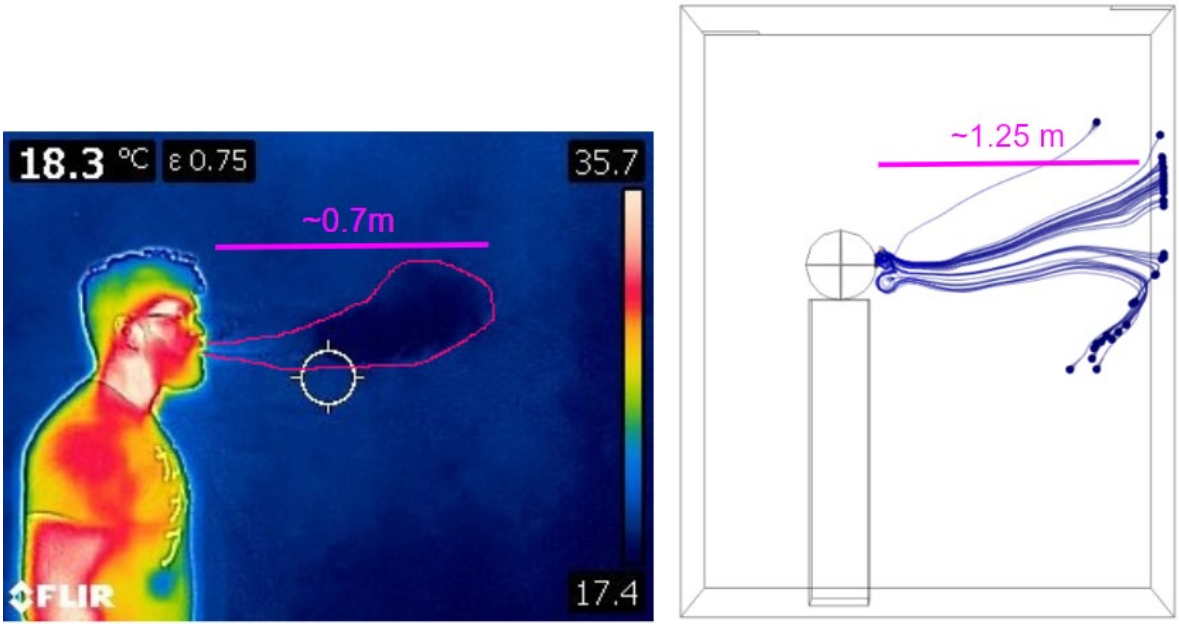

Figures 22a and 22b: Shallow breathing with no inlet vent

As observed in Fig. 22a and 22b, the direction and dispersion of the particles in the simulated plot is like that of experimental data. In both scenarios, the plume starts out narrow and widens as it gets farther from the source. The particles traveled farther overall in the simulated computation than in the thermal imaging experiment, but the overall trajectories and patterns of dispersion are very similar. The discrepancy can be attributed to differences in mouth geometry as well as ambient flow in the experimental setup.

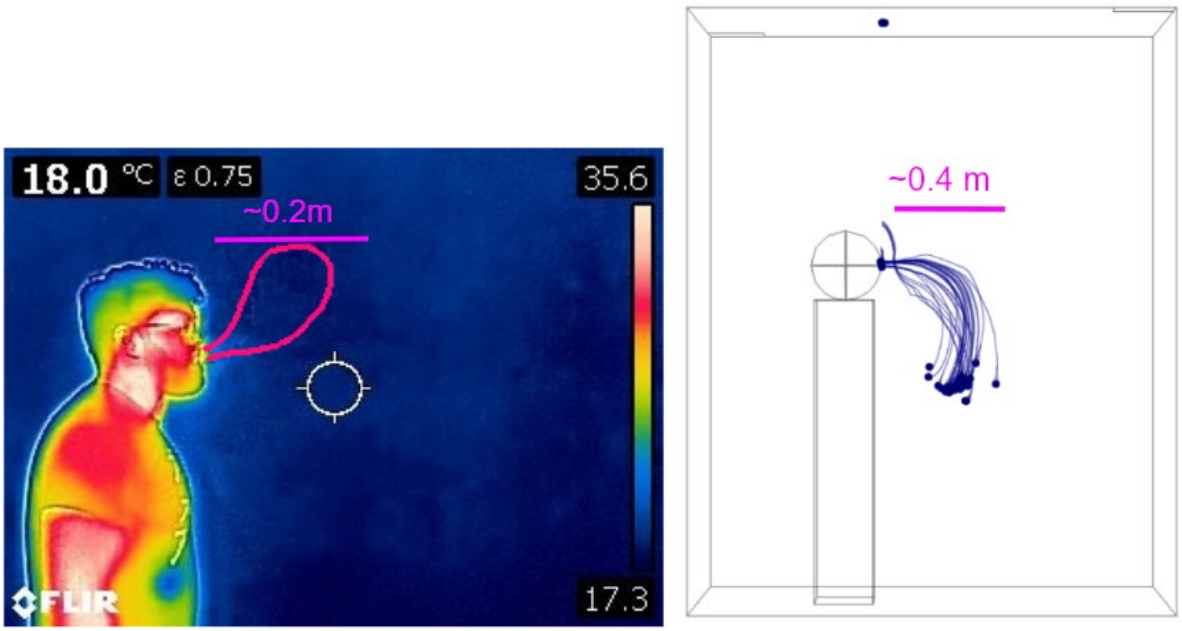

Figures 23a and 23b: Deep breathing with no inlet vent.

For deep breathing, the direction and path of propagation of the two simulations is similar to that of the experimental data for. In Figures 23a and 23b, the data recorded thermal imaging camera indicates that the particles propagate upwards until they are at maximum 0.2 m away from the breathing inlet. The simulation recorded a similar phenomenon, but with a distance of 0.4 m and a downward trajectory. The difference in the propagation patterns is most likely due to the effects of convective heat transfer in the thermal images. The thermal convection currents generated by body heat is enough to carry the particles upwards, especially because the particles are released with a lower velocity from the mouth (as per the deep breathing function). Additionally, once the particles reach room temperature they are no longer visible on the plot. This explains the shorter distance of propagation in both shallow and deep breathing thermal imaging plots as the particles likely travelled further but the camera could only capture a short amount of this propagation. Despite the small discrepancy between the experimental data and the model results, the general trend of the particle trajectories is similar, and thus serves to validate our breathing functions. Ideal experiments would simulate the entire elevator volume with both inlet and outlet vents.

Sensitivity Analysis:

The initial calculation centered on the schematic involving a person staying stationary in an empty elevator towards the middle back. By varying the location of the person around the elevator, the difference in particle velocities and total distance of propagation 35 seconds after release from 5 different coordinate locations was analyzed. 35 seconds was chosen as the time to analyze the distances to simulate a short elevator ride.

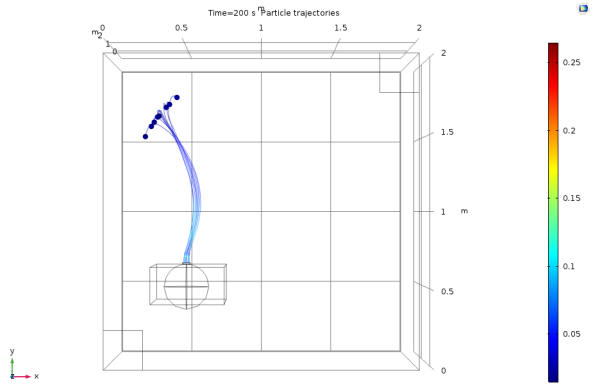

Figure 24a: Trajectories at (.5, .5)

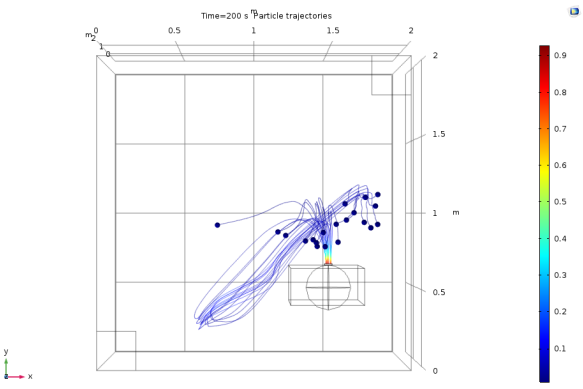

Figure 24b: Trajectories at (1.5, .5)

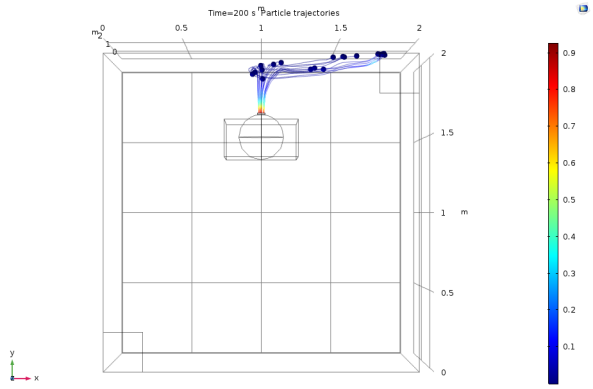

Figure 24c: Trajectories at (1, 1.5)

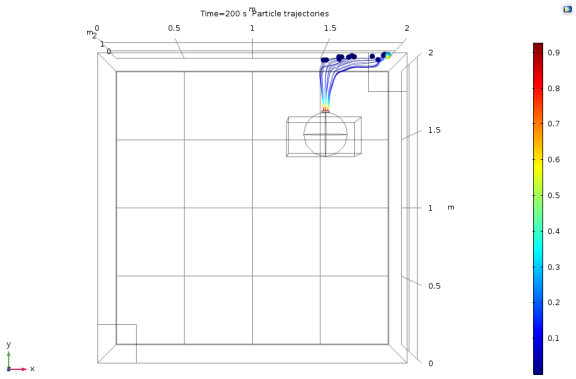

Figure 24d: Trajectories at (1.5, 1.5)

As shown by the plots of particle trajectories for varying source positions, the position of the source has a wide impact on particle position and velocity.

The average distance of propagation and velocity for the normal solution and 4 variations 35 seconds after release were also plotted:

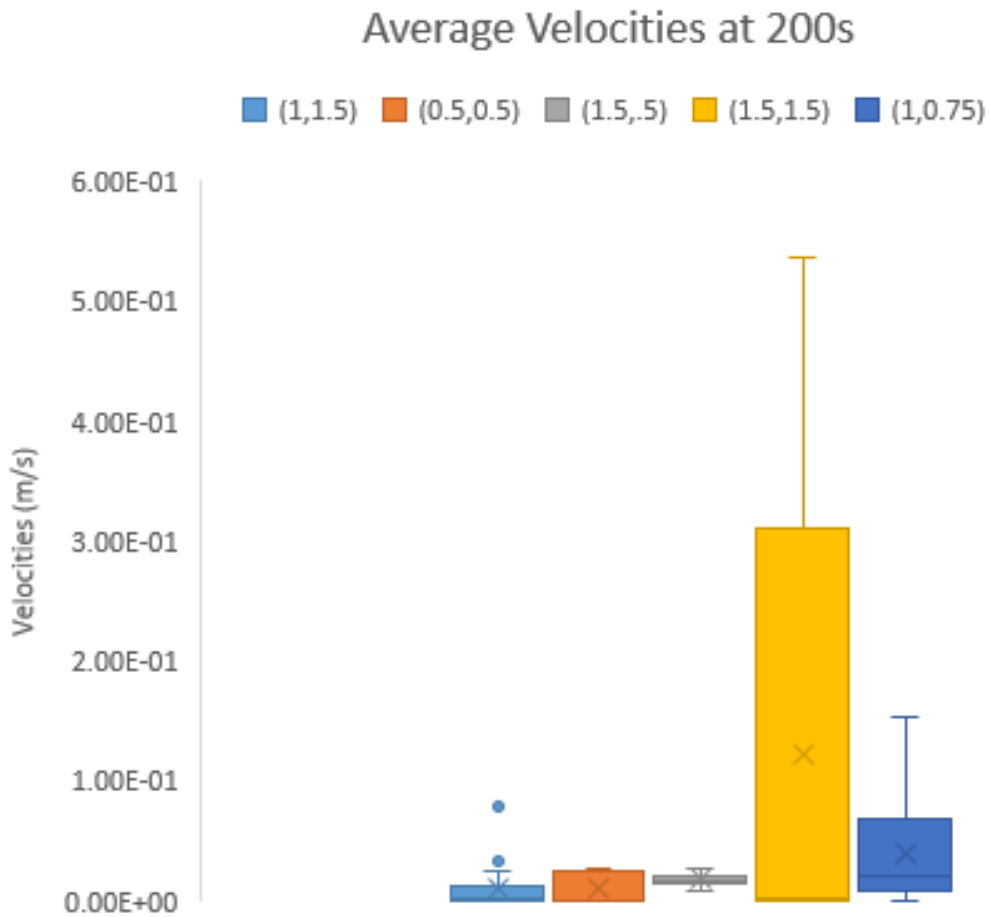

Figure 25: Average velocity of particles. For most variations, the particle velocities at 200 seconds were close to 0, due to the fact that most of the particles had stuck to the walls by this time. The (1.5,1.5) variation is the only one that had significant numbers of particles experiencing non zero velocities due to the fact that these particles were still floating in the elevator at 200 seconds.

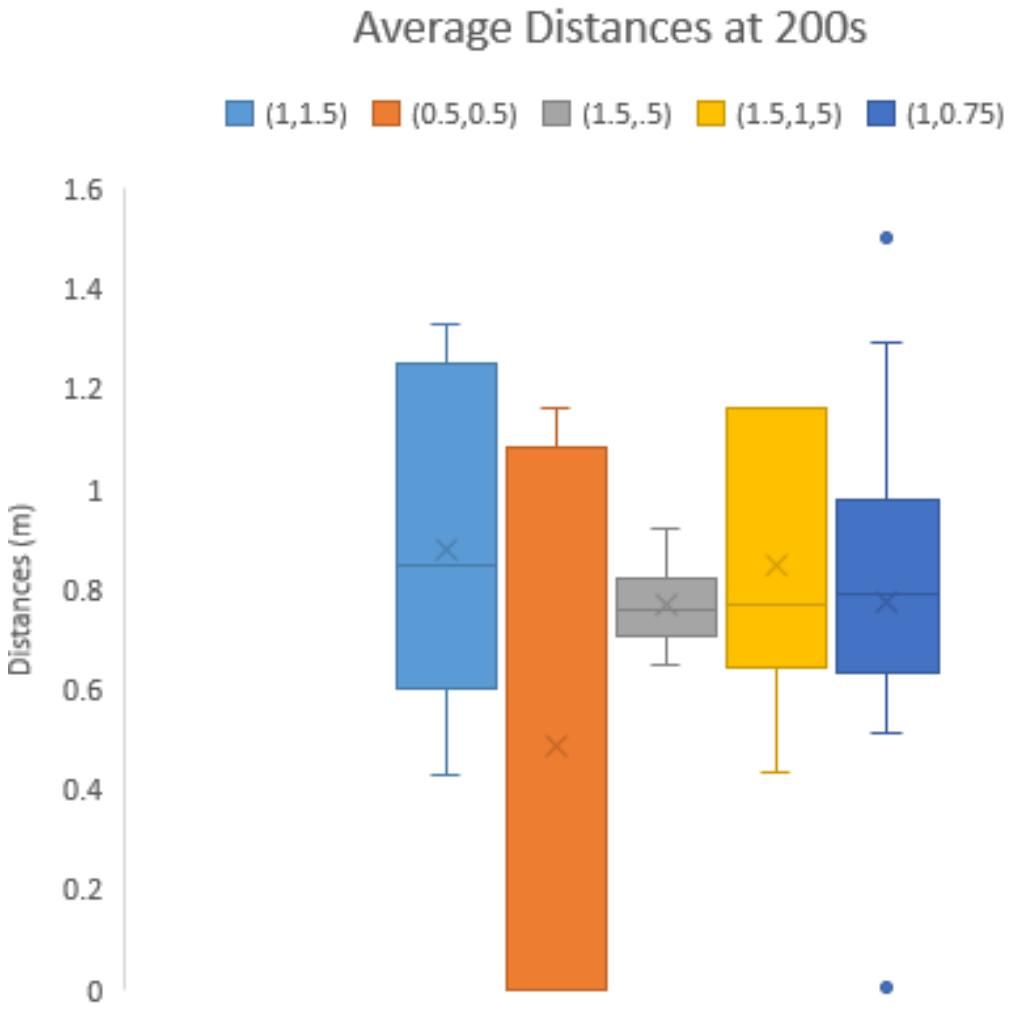

Figure 26: Average distance of propagation from the source. This figure illustrates that for certain source positions, not only is the average distance lower, but the distribution of particle positions is smaller. This can be explained by the particles emitted close to the wall sticking directly to the wall, and particles emitted near the outlet vent being quickly sucked into the outlet without having time to disperse.

As indicated by Fig. 26, the particles released by the person at (1.5, 1.5), or the closest position to the outlet have a much larger spread in velocity than the other positions after 35s. This pattern is explained by the proximity to the vent--the particles travel directly towards the vent and many are close to the outlet after 35 s. The “head start” experienced by those released closest to the outlet means that they speed up more due to the increasing velocity field close to the vent.

Similarly, the particles release furthest from the outlet (.5, .5), experienced a much larger spread of total propagation distance than those released at other positions. This is in part due to some particles sticking to the surfaces close to the mouth, but also because they don't experience as large a pull from the outlet vent as the other releases, and therefore are in a section with a more moderate velocity gradient. They also seemed to exhibit the same pattern of backwards flow as seen in the normal solution, where the particles released in the upper half of the schematic close to the outlet do not. This could indicate an eddy pattern that exists only in the lower left quadrant of the schematic diagram.

The breathing function was also varied to simulate deeper breathing patterns and shallower breathing patterns. The shallow breathing function had a maximum velocity of 1.8 $\frac{m}{s}$ and a period of 2 seconds, while the deep breathing function had a maximum velocity of .6 $\frac{m}{s}$ and a period of 6 seconds. The particles were released in the same manner as the initial computation, starting at 40 seconds. The results for particle trajectories after 100 seconds of computation are seen below.

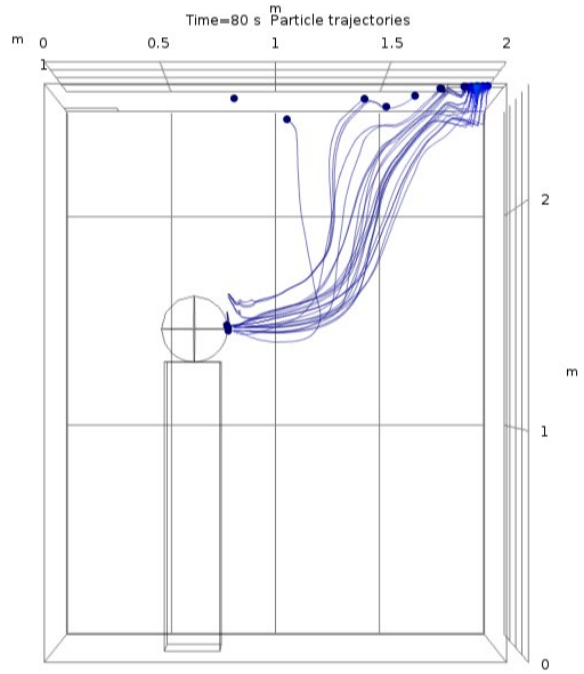

Fig. 27a: Shallow Breathing particle trajectories

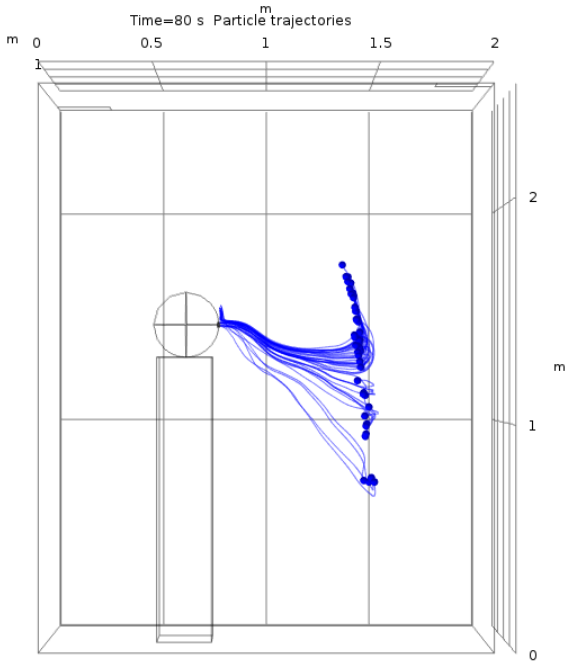

Fig. 27b: Deep Breathing particle trajectories

As seen in the figures above, the particles that were released using a shallower breathing function initially moved towards the vent without being drawn towards the eddy that the particles in the initial computation experienced. The slower and deeper breathing pattern showed that the particles followed a similar trajectory as the initial computation, moving first towards the outlet, before experiencing backflow towards the inlet vent. This indicates that a shallower and quicker

breathing pattern allows the particles to experience sufficient initial velocity to surpass the eddy currents that trap the particles in deep and normal breathing patterns into a backflow and cyclical propagation pattern. The deep breathing function did not create a significant enough velocity gradient to prevent the particles from experiencing the full complexity of the fluid flow characteristics near the wall.

To analyze this phenomena further, the average distance of propagation at 100 seconds of the normal breathing pattern, the shallow breathing pattern, and the deep breathing pattern were plotted.

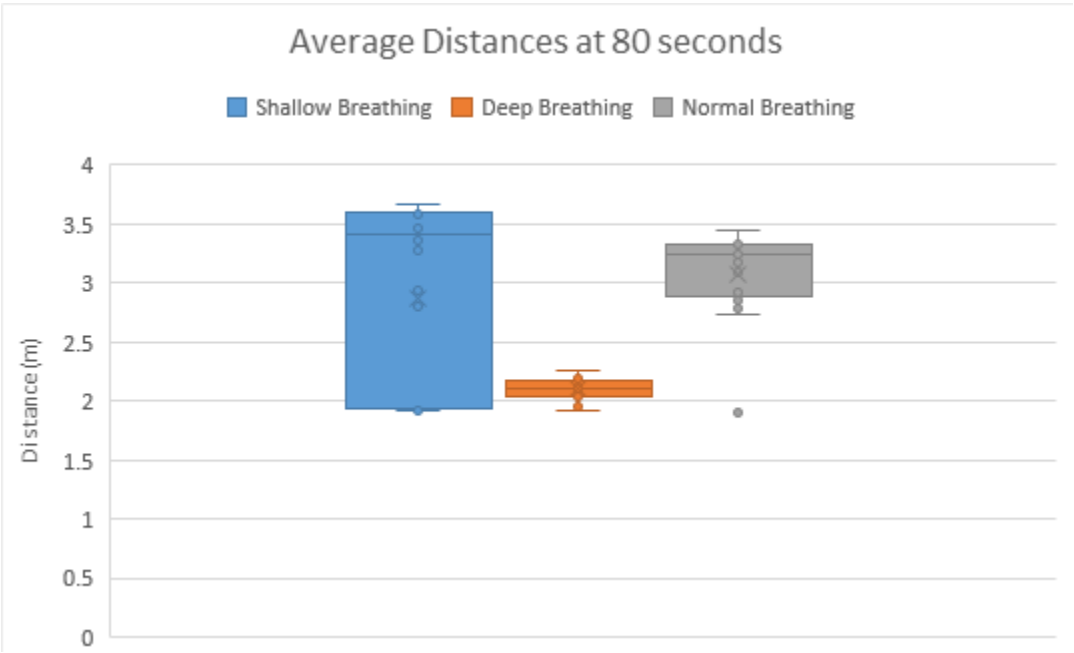

Figure 28: the average distance of propagation at 100 seconds for different breathing functions. The deep breathing function shows a much smaller average distance traveled (and a smaller spread) due to being trapped in eddy currents. The particles released during shallow breathing on the other hand, bypass the eddy currents and move nearly directly into the outlet vent.

As seen in the figure above, the spread and average distance of the particles released using a shallow breathing function is larger than that of normal or deep 35 seconds after release. This is closely followed by normal breathing, but the particles released using a deep breathing function spread less overall as well as remained closer to the mouth than the other two functions. This indicates that the stronger and quicker the breathing pattern, the quicker the particles will spread, and the farther they will travel, but in this case meant that they would travel into the outlet vent faster.

This research also explored the effects of changing the particle diameter on the final solution at 100 seconds. There was no change in results between diameter values of .5-18 μm, and so it is

valid to conclude that varying particle diameter does not significantly affect the propagation or velocity of the particles when remaining within a small range of particle size.

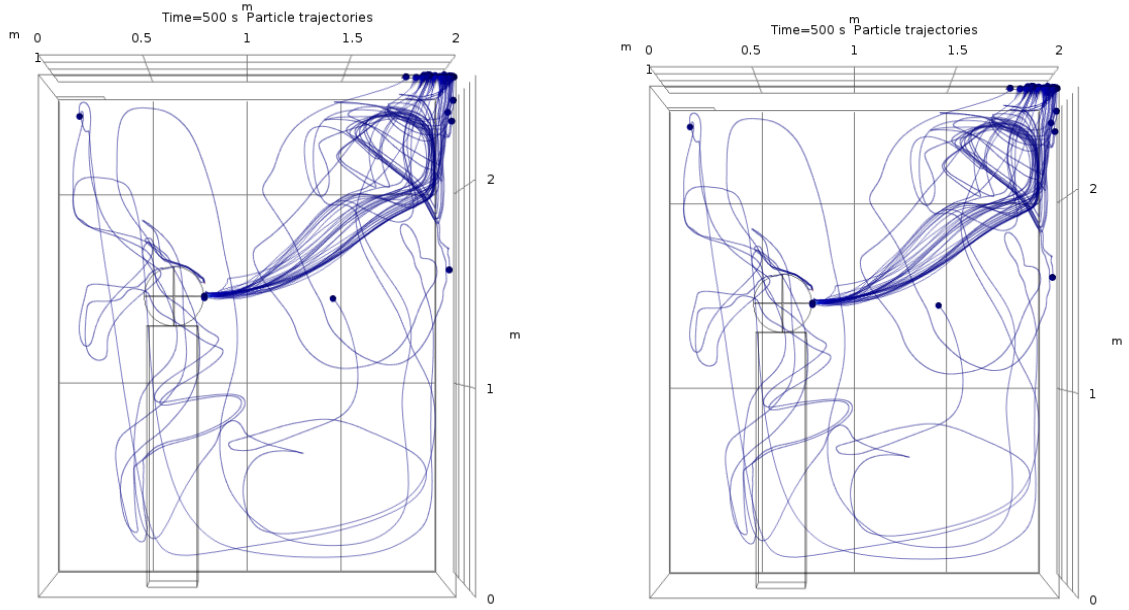

Figures 28a and 28b: The dispersion of particles of 0.5 μm diameter (left) and 18 μm diameter (right)

The system was also analyzed with a low inlet velocity (0.2 $\frac{m}{s}$), medium (0.7$\frac{m}{s}$) and a high inlet velocity (1 $\frac{m}{s}$). The particle trajectories after 80 seconds are shown in the plots below.

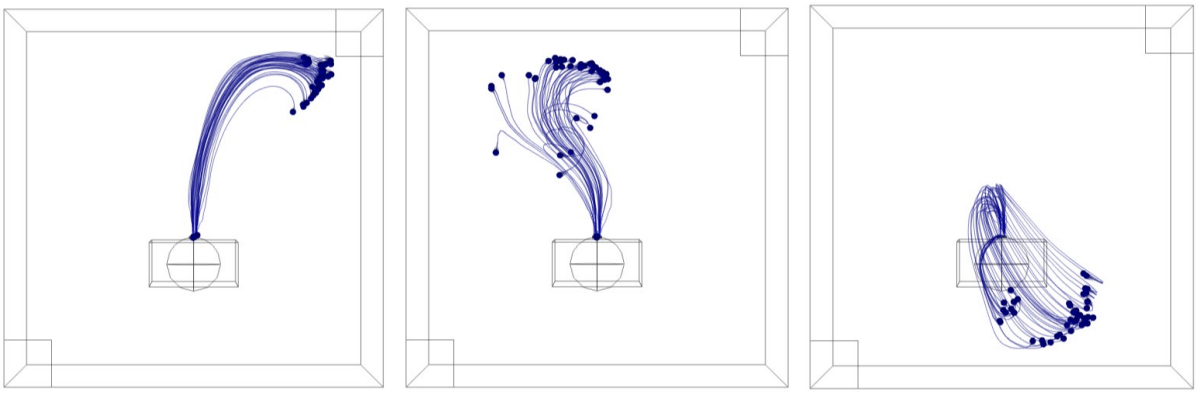

Figures 29a, 29b, 29c: From left to right: Low inlet velocity (0.2 $\frac{m}{s}$), Medium inlet velocity (0.7 $\frac{m}{s}$), High inlet velocity (1 $\frac{m}{s}$)

Upon initial inspection it appears that the variation of inlet velocity has a large effect on particle dispersion, and that velocity has an inverse effect on the rate of fluid exchange in the elevator. This is further evidenced by the high inlet velocity causing significant backflow and turbulence almost immediately after release, with the low inlet velocity creating a smooth and even

propagation of particles towards the outlet vent. The medium inlet velocity causes a flow pattern of somewhere in the middle, causing neither significant turbulence nor effecting an even and straightforward flow pattern towards the vent.

However, at longer times, the particles released with a low inlet vent velocity don't continue to propagate towards the vent: they experience a backflow that brings them closer to the initial release point, and then they slowly circulate towards the outlet vent while following the same cyclical and radially expanding streamlines many of the other variations experience. This indicates that while at small times a low inlet velocity can decrease the spread of particles, after longer times a lower inlet velocity ensures that the fluid complexities experienced by the other simulations will simply happen later in the simulation. This means a longer period of circulation for the infectious particles, increasing the likelihood of contamination over time.

This is corroborated by the plot below showing the number of infectious particles left in the elevator over time for each of the inlet speeds.

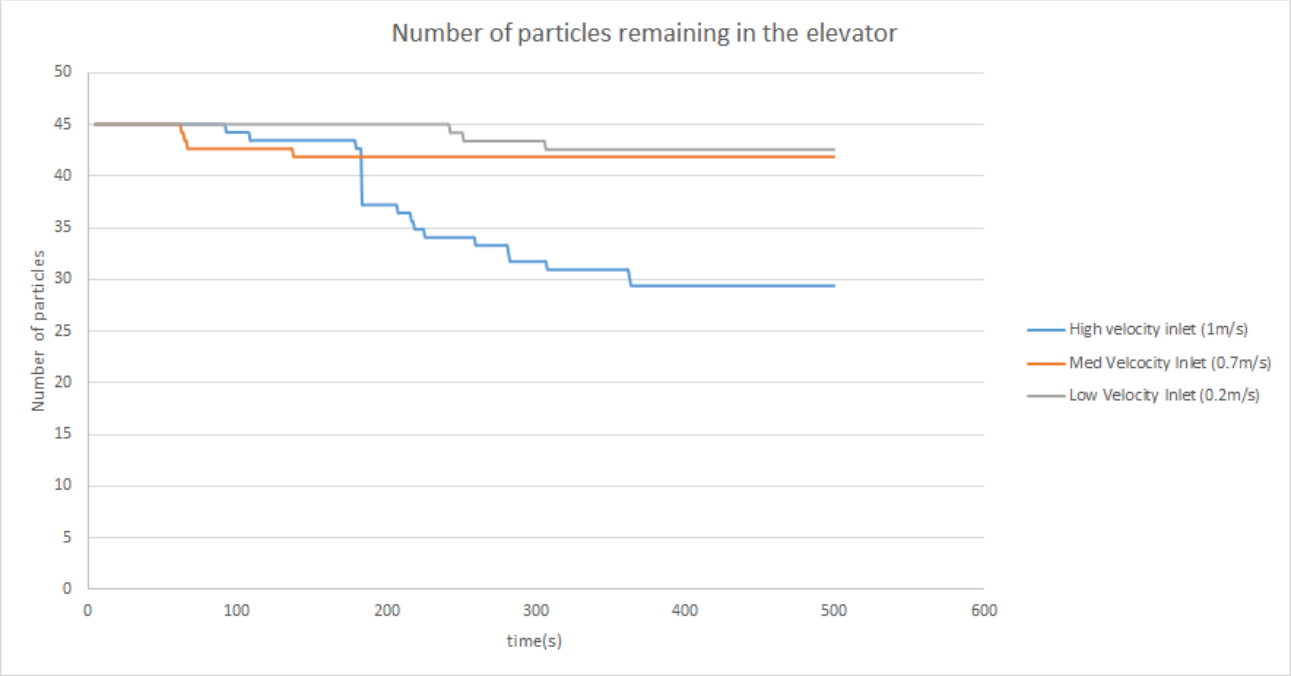

Figure 30: The number of particles remaining the sample space over time. This data was collected by evaluating the probability that any particles was stuck in the vent at any certain time, which was given as a ratio of the number of particles stuck in the vent to the total number of particles.

As shown by Fig. 30, the highest inlet velocity led to the largest number of particles sucked out of the outlet vent, but only after around 100 - 150 seconds. Before this time, the number of particles remaining in the space is similar for all inlet velocities. This data is important as it

shows that for longer elevator rides, increasing the inlet velocity does decrease the number of particles in the elevator over time, however for shorter rides this has little effect. This is because regardless of the inlet velocity, the particles will be caught in some eddy flow for a period of time after release. Variation of inlet velocity can be considered as a design parameter to reduce contamination, but the effects will only be seen after the time when the particles exit the circulation caused by the initial backflow patterns.

7. Conclusion

The results show that there are a wide variety of factors that contribute to the distribution of particles in a given model. Among the most important were the location of the body in the elevator, and breathing pattern. The most significant impact of the variation of those parameters is the time of circulation. If the particles enter into a backflow or a fluid eddy, they don't come to rest for far longer than if they propagate straight towards the vent, meaning they have the ability to contaminate a larger area of space over time.

Indicated by the sensitivity analysis are several parameters that have a large effect on fluid complexities, backflows, and eddies. These include the distance between the source of propagation and the outlet vent, the rate of flow of the inlet vent, and the function of breathing overall. To reduce the chances of contamination over time by long elevator rides by increasing fluid exchange, higher inlet velocities could be incorporated as well as more or larger outlet vents, closer to the particle source. Of these two design considerations, decreasing the distance between any person and an outlet vents would have the largest effect on the final deposition of particles.

Further research is needed to analyze the effects on flow of increasing the number of people in an elevator. Because the fluid characteristics of the model varied so drastically based on where the person was in relation to the vent flow pattern, it is likely that increasing the number of people in the elevator and adding a more complex schematic will increase the turbulence of the flow and have a large effect on time of particle circulation. Specific modeling with greater complexity is necessary before any final design recommendations could be made for any set geometry.

This model can be further refined to help determine the optimal design parameters for a specific geometry to reduce airborne disease transmission.

5. References

Al-Kodmany, K. (2015). Tall Buildings and Elevators: A Review of Recent Technological Advances. *Buildings*. https://doi.org/10.3390/buildings5031070

Christian, M. D., Loutfy, M., McDonald, L. C., Martinez, K. F., Ofner, M., Wong, T., … Low, D. E. (2004). Possible SARS Coronavirus Transmission during Cardiopulmonary Resuscitation. *Emerging Infectious Diseases*. https://doi.org/10.3201/eid1002.030700

Fryar, C. D., Kruszon-Moran, D., Gu, Q., & Ogden, C. L. (2018). Mean Body Weight, Height, Waist Circumference, and Body Mass Index Among Adults: United States, 1999-2000 Through 2015-2016. *National Health Statistics Reports*.

International Building Code, Chapter 30 Elevators and Conveying Systems ξξ Section 3004.1-3004.4 (2012)

International Building Code, Chapter 4 Ventilation ξξ Section 403 Table 403.3.1.1 (2015)

Jones, R. M., & Brosseau, L. M. (2015). Aerosol transmission of infectious disease. *Journal of Occupational and Environmental Medicine*. https://doi.org/10.1097/JOM.0000000000000448

Kandel, C. E., Simor, A. E., & Redelmeier, D. A. (2014). Elevator buttons as unrecognized sources of bacterial colonization in hospitals. *Open Medicine*.

Nazaroff, W. W., & Cass, G. R. (1989). Mass-transport aspects of pollutant removal at indoor surfaces. *Environment International*. https://doi.org/10.1016/0160-4120(89)90078-0

Tang, J. W., Nicolle, A. D., Klettner, C. A., Pantelic, J., Wang, L., Suhaimi, A. Bin, … Tham, K. W. (2013). Airflow Dynamics of Human Jets: Sneezing and Breathing - Potential Sources of Infectious Aerosols. *PLoS ONE*. https://doi.org/10.1371/journal.pone.0059970

Thomas, R. J. (2013). Particle size and pathogenicity in the respiratory tract. *Virulence*. https://doi.org/10.4161/viru.27172

Yan, Y., Li, X., Shang, Y., & Tu, J. (2017). Evaluation of airborne disease infection risks in an airliner cabin using the Lagrangian-based Wells-Riley approach. *Building and Environment*. https://doi.org/10.1016/j.buildenv.2017.05.013

Zhao, B., Zhang, Z., & Li, X. (2005). Numerical study of the transport of droplets or particles generated by respiratory system indoors. *Building and Environment*. https://doi.org/10.1016/j.buildenv.2004.09.018

6. Appendix

A. Input Parameters (shown in governing equations, page 16-17)

Property	Symbol	Value	Source
Surface gravity	g	9.8 m/s^2	COMSOL
Air density	ρ	1.229 kg/m^3	COMSOL
Air viscosity	μ	1.81×10^{-5} kg/(m. s)	COMSOL
Particle density	ρ_p	1000 kg/m^3	COMSOL (density of

			water)
Particle Diameter	d_p	1.8 μm	Thomas et al.
Particle velocity	v	Solved for in particle tracking	Solved for
Fluid velocity	u	Solved for in fluid flow	Solved for

B. Additional Figures

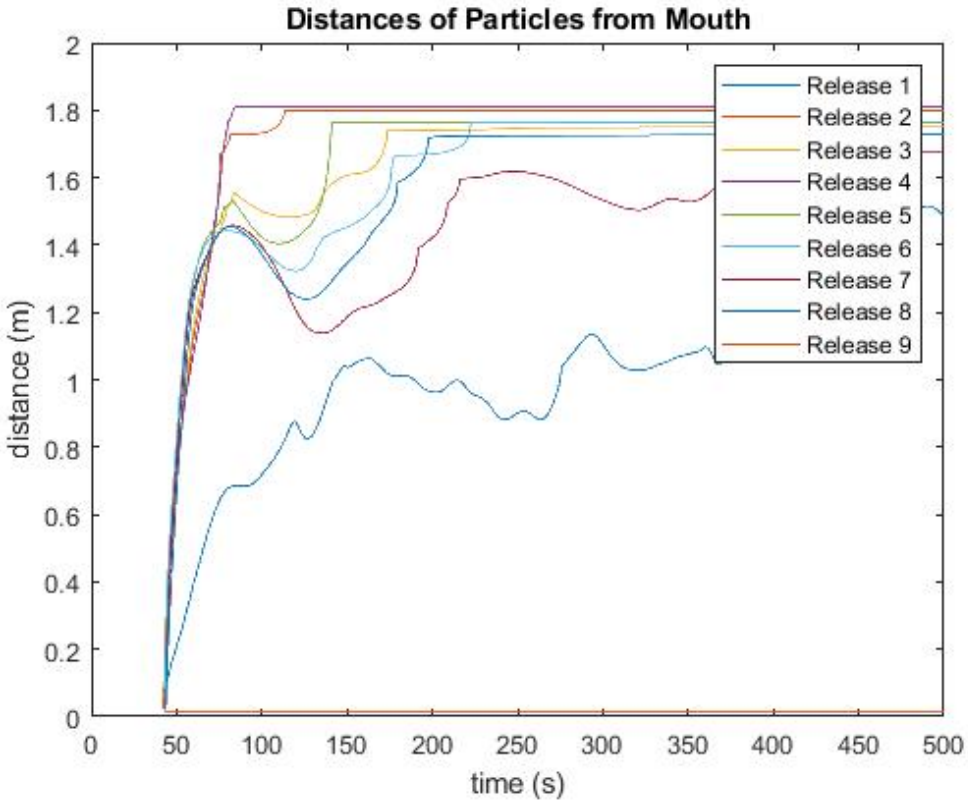

Figure 1: Total propagation distance over time by particle, one particle per release

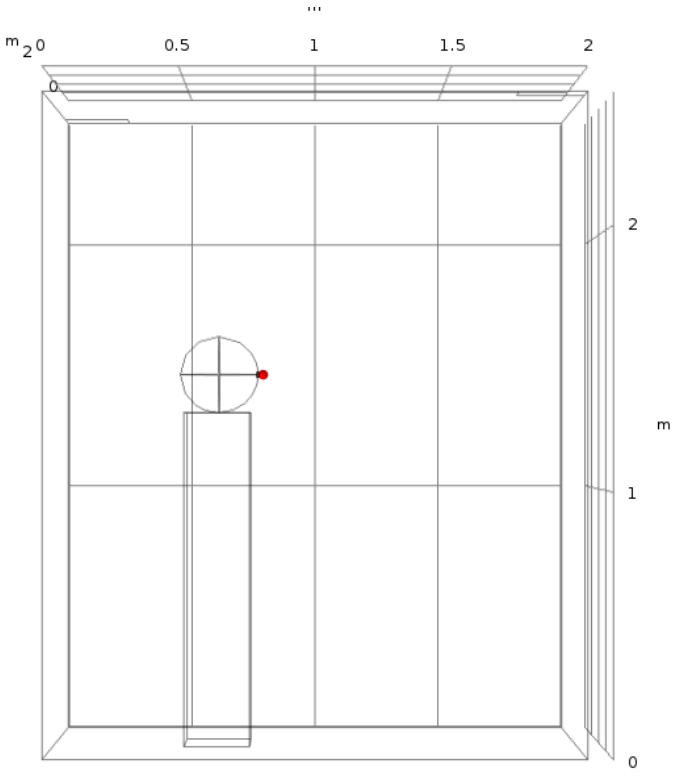

Figure 2: Cut point for Mesh Convergence

C. Computational time taken for a single run of fine mesh model computing Laminar Flow

```
Time-stepping completed.
Solution time: 1037 s. (17 minutes, 17 seconds)
Physical memory: 1.67 GB
Virtual memory: 1.98 GB
Ended at 7-May-2019 01:49:18.
----- Time-Dependent Solver 1 in Study 1/Solution 1 (sol1) ---------------------->
================================================================================
```

D. Computational time taken for a single run of fine mesh model computing Particle Tracking

```
Solution time: 323 s. (5 minutes, 23 seconds)
Physical memory: 1.38 GB
Virtual memory: 1.61 GB
Ended at 7-May-2019 02:12:45.
----- Time-Dependent Solver 1 in Solution 2 (sol2) ---------------------------->
================================================================================
```

E. Team Responsibilities

Team member name	Rae Brigham	Yohan Sequeira	Meghana Machireddy
Wrote abstract	X	X	X
Edited abstract	X	X	X
Wrote introduction		X	
Edited introduction		X	X
Wrote method section	X	X	X
Edited method section	X	X	X
Wrote results section	X	X	X
Edited results section	X	X	X
Wrote discussion section	X	X	X
Edited discussion section	X	X	X
Wrote summary and conclusion section	X	X	
Edited summary and conclusion section	X	X	X
Wrote bibliography section	X		
Edited bibliography section	X	X	X
Prepared processed data table for appendix	X	X	X
Checked data in processed data table in appendix	X	X	X
Prepared figures or tables for main text	X	X	X
Checked figures or tables in main text	X	X	X
Assigned tasks to group members	X	X	X
Put the report together from the parts provided by others	X	X	
Read and edited entire document to check for consistency	X	X	X